OPEN ACCESS

Oligoether Ester-Functionalized ProDOT Copolymers on Si/Monolayer Graphene as Capacitive Thin Film Electrodes

To cite this article: Tolga Karazehir *et al* 2020 *J. Electrochem. Soc.* **167** 070543

Journal of The Electrochemical Society, 2020 **167** 070543

Oligoether Ester-Functionalized ProDOT Copolymers on Si/Monolayer Graphene as Capacitive Thin Film Electrodes

Tolga Karazehir,[1,z] Baran Sarac,[2] Hans-Detlev Gilsing,[3] Jürgen Eckert,[2,4] and A. Sezai Sarac[5]

[1]*Department of Energy System Engineering, Adana Alparslan Türkeş Science and Technology University, 01250 Saricam, Adana, Turkey*
[2]*Erich Schmid Institute of Materials Science, Austrian Academy of Sciences, 8700 Leoben, Austria*
[3]*Institute of Thin Film and Microsensoric Technology (IDM), 14513-Teltow, Germany*
[4]*Department of Materials Science, Chair of Materials Physics, Montanuniversität Leoben, 8700 Leoben, Austria*
[5]*Polymer Science and Technology, Nanoscience & Nanoengineering, Istanbul Technical University, 34469 Istanbul, Turkey*

In this study, electrochemical polymerization of 3,4-propylenedioxythiophene (ProDOT **1**), ProDOT bearing oligoether ester (ProDOT-EO-ester **2**) and their copolymerization onto homogeneously CVD coated nano-graphene/Si support is realized to attain graphene/ProDOT based copolymer hybrid nanostructures. By introducing oligoether side chain to ProDOT backbone and using different [ProDOT]/[ProDOT-EO-ester] molar ratios ensures a considerable decrease in oxidation potential of polymer allowing tunable properties to copolymers revealing improvement electrochemical capacitance and electrochemical activity which are clearly reflected by the experimental results. Capacitive behavior of copolymers is determined by electrochemical impedance spectroscopy, cyclic voltammetry. Moreover, The structural, morphological and spectroscopic characterization of the copolymers is investigated by XRD, AFM, SEM, EDX, FTIR, and Raman, respectively. By the increase of ProDOT in the copolymer composition, the higher dopant concentration is attained suggesting an enhanced conductivity agree well with the impedance and CV results, where the copolymerization of ProDOT **1** and ProDOT-EO-ester **2** in equal molarity results in the highest specific capacitance and redox activity. The adopted equivalent circuit model for polymers is in good agreement with the experimental data of impedance. Due to the difference in conjugated structure between ProDOT and ProDOT-EO-ester by the presence of the EO-ester group leads to a decrease in charge transfer resistance with increasing mole fraction of ProDOT-EO-ester. The charge transfer resistance of $[ProDOT]_0/[ProDOT\text{-}EO\text{-}ester]_0 = 1{:}1$ coated Si/graphene is nearly 51 and 24 times lower value compared to those of PProDOT and P(ProDOT-EO-ester) homopolymers coated Si/graphene, respectively, confirming that the copolymerization improves the electron conduction. By Mott-Schottky measurements, increasing mole fraction of ProDOT-EO-ester **2** in copolymer composition results in the alteration of semiconducting behavior. The developed graphene-polymer hybrid electrodes can be a potential candidate for energy storage devices.
 [DOI: 10.1149/1945-7111/ab7f85]

Manuscript submitted January 1, 2020; revised manuscript received February 27, 2020. Published March 23, 2020. *This paper is part of the JES Focus Issue on Challenges in Novel Electrolytes, Organic Materials, and Innovative Chemistries for Batteries in Honor of Michel Armand.*

Supplementary material for this article is available online

Electrically conductive carbon allotropes can either be modified by polymer coating or, after oxidative functionalization by combination with metal oxide particles generating different types of derivatives with various morphologies and porosities. Thus, these carbon-based matrices have received great attention as components of electrode materials for energy storage devices.[1–8] Graphene as a two dimensional allotropic form of *carbon* exhibits unique properties such as high electronic mobility and thermal conductivity, very low electric resistance, large specific surface area, optical transparency, and high mechanical strength, respectively.[9,10] Due to long-term stability and low production cost, graphene-based composites have been introduced as supercapacitor materials.[11–16]

According to the properties of the electrode material, two mechanisms of charge storage can be distinguished.[17–19] In the case of non-redox active materials, the electrodes are surrounded more and less densely by electrostatically attracted solvated ions forming electrical double layers and charge storage is taking place only by non-faradaic processes of ion adsorption and desorption at the electrodes and the interface to the electrolyte layer, respectively. These systems are called electrical double-layer capacitors (EDLCs). On the contrary, charge storage at redox-active electrodes involves electron transfer processes; electrochemical capacitors of that type are classified as pseudocapacitors.[20] Supercapacitors have higher power densities than other energy storage devices and can be charged and discharged quickly for multiple times, but store only lower magnitudes of energy than batteries.[21] Therefore, new electrode materials for enhancement properties of the supercapacitor are important to provide desirable cycle life, capacitance, energy and power density.[22]

Graphene as a typical supercapacitor material has been combined with conducting polymers like poly-aniline,[23,24] polypyrrole[25–27] and poly(3,4-ethylenedioxythiophene) (PEDOT),[28–31]. Composites of PEDOT and graphene can be prepared by noncovalent π-π interactions,[32] and in situ polymerization,[33] electrochemical polymerization,[34] and vapor phase polymerization.[35]

Among conducting polymers, especially for redox applications, 3,4-alkylenedioxythiophene have advantages over thiophene analogs due to its structural unit containing two electron-donating oxygen atoms in 3- and 4-position of the heterocycle and a rigid ethylene ether bridge. PEDOT is characterized by a low oxidation potential, moderate band-gap, good conductivity, high chemical stability and reversibility of switching, which has led to successful commercialization inducing various applications.[36,37] 3,4-proylenedioxythiophene (ProDOT) have two reactive hydrogens (at the 2- and 5- positions) and modification of the molecule is possible by introduction of a functional group at the 2-position of the propylene bridge.[38] For expansion of the synthetic flexibility of the monomer and side chain engineering in the polymer structure a number of functionalized derivatives structurally related to ProDOT have been developed.[39] In the previous studies, diester-substituted ProDOT derivative introduced as the cathodically coloring electrochromic polymers switching from a deep purple to a highly transmissive gray/blue.[40] ProDOT based conjugated polymer produced via

[z]E-mail: tkarazehir@atu.edu.tr

electrochemical polymerization with diethyl malonate pendant group was reported to realize the navy color of the polymer film.[41] Oligoether (oligo(oxyethylene)) and ester-functionalized ProDOT based polymer, where alkali metal ion coordinating oligoether units and a reactive ester group in the side chain, was studied for ion sensors.[42] It was shown that the electrochemical polymerization of the oligo(oxyethylene)-substituted polymer reveals a negative shift of the oxidation potential and a significant enhancement of the effective conjugation length with a 0.10 eV decrease of the bandgap.[43] In addition, carbon-based electrodes electrochemically coated by PProDOTs bearing alkyl and alkyl-aryl groups[44–49] or polar functional groups[50,51] show improved capacitive behavior. Recently, PProDOT copolymers carrying oligoether or carboxylic acid functional groups[52,53] were identified for the improvement of the solubility and processability, and were utilized as materials of high capacitance on carbon electrodes. The presence of an oligoether chain or a carboxylic group additionally allows coating processes of an electrode with chemically prepared PProDOTs from organic solvents or with carboxylic salt from aqueous solution.

Electropolymerization is a simple, practical and inexpensive way to generate desired surface structures of modified electrodes for various applications.[54–57] This technique ensures full control of the surface morphology, electrical conductivity, and electroactivity by modifying the monomer chemistry or the electrochemical parameters. As a consequence, by changing these set screws, it is possible to fine-tune the surface structures and to provide favored semiconducting properties.

In this manuscript, starting from a brief description of the types of carbon-based electrodes for energy storage devices, the properties of graphene and the application of its composites as a supercapacitor material are explained. Due to the different types of supercapacitors (EDLCs and pseudocapacitors), the idea of coating graphene by a suitable conducting polymer to enhance capacitance by pseudo-capacitive redox reactions is deduced. After the presentation of PEDOT as modifying component of graphene composite electrodes development of the structural analogue PProDOT is discussed, and the capacitive behavior of carbon-based electrodes coated by PProDOT derivatives is elucidated. There from, the experimental approach of the paper to use ProDOT/ProDOT-EO-Ester copolymers combining structural elements of ProDOT copolymers from the literature exhibiting excellent capacitive behavior is developed. For clarification purposes, the chemical structures of ProDOT and ProDOT-EO-Ester were explicitly shown in the Fig. S1 (available online at stacks.iop.org/JES/167/070543/mmedia). Here, the addition of EO-ester functionality confers sufficient low oxidation potential for copolymerization to provide an enhanced redox activity and capacitance properties. Different ratios of ProDOT-EO-ester to ProDOT were copolymerized yielding the copolymers herein referred to as CP1-1, CP1-5, CP1-25, and CP1-50, electrodeposited onto homogeneously CVD coated nanographene/Si support for the purpose of development of new graphene/ProDOT hybrids.

Experimental

Materials.—3,4-Propylenedioxythiophene **1** (ProDOT, 97%) and tetraethylammonium tetrafluoroborate (Et_4NBF_4, 99%) were purchased from Sigma Aldrich and used without further purification. Acetonitrile and dichloromethane (Sigma-Aldrich) were of analytical grade. CVD-grown monolayer graphene film on B doped SiO_2/Si substrate (transparency; >97%, coverage; >95%, number of graphene layers; 1, thickness (theoretical); 0.345 nm, Hall electron mobility on SiO_2/Si; 2000–3500 $cm^2\ Vs^{-1}$, sheet resistance on SiO_2/Si (Van der Pauw); 450 ± 40 Ohms $sq.^{-1}$ for 1 cm × 1 cm) was purchased from Graphenea. ProDOT-EO-ester **2** was synthesized as reported previously.[42] Table I summarizes the distribution of ProDOT **1** and ProDOT-EO-ester **2** and copolymers. χ is the mole fraction of ProDOT 1 monomer.

Methods.—Electrocopolymerizations were performed by cyclic voltammetry (CV) using a Princeton Research potentiostat/galvanostat (Parstat 4000A) with a Versa Studio software package. The monolayer graphene (0.345 nm) on SiO_2/Si, produced by chemical vapor deposition (CVD) and transferred to a substrate of SiO_2/Si (300 μm) by a wet transfer process, was purchased from Graphenea. The content of monolayer graphene is constant during the electrodeposition of homopolymers or copolymers onto the monolayer graphene-modified silicon wafer, whereas the content of copolymer is varied by using different monomer feed ratio. A three-electrode system was employed. Monolayer graphene-coated Si wafer was used as the working electrode, Ag/AgCl (3 M NaCl/Saturated AgCl), where its redox potential is +0.209 V vs. standard hydrogen electrode at 25 °C as the reference electrode, and platinum wire as the counter electrode. Electrochemical impedance spectroscopy (EIS) measurements were performed to observe electrical properties of each homopolymer and copolymer coated Si/graphene electrodes at room temperature by Parstat 4000A potentiostat/galvanostat which is configured with a conventional three-electrode cell at open circuit potential (OCP) condition in 0.1 M Et_4NBF_4/ACN:DCM (3:1) solution. Frequency range was between 10 mHz and 100 kHz, and the applied AC signal amplitude was 10 mV. The ZSimpWin V 3.10, an AC impedance data analysis software, was provided to fit appropriate equivalent circuit model for modeling the impedance spectra. Structural analysis of the polymer coated Si/Graphene electrodes was performed using Fourier transform infrared- Attenuated total reflectance spectroscopy (FTIR-ATR) (Bruker Vertex 70 ATR) in the range of 400–4000 cm^{-1}. Raman spectroscopy (DXR Raman spectrometer (Thermo Scientific, Massachusetts, USA)) was applied at 532 nm, and X-ray diffraction analysis (XRD) including the grazing incidence mode by Rigaku SmartLab 5-Axis X-ray diffractometer with Co Kα radiation was performed for copolymer and homopolymer coated nanographene/Si substrates. Scanning Electron Microscopy (SEM) images (Gemini Leo Supra 35 VP) and energy dispersive X-ray (EDX) analysis attached to SEM was performed for copolymer and homopolymer coated monolayer graphene/Si substrates. AFM analysis was carried out using a Nanoscope ezAFM+ with a cantilever tip radius of 10 nm. The images were obtained using the non-contact mode of AFM. The Mott–Schottky (M–S) experiments were conducted to determine the semiconducting properties of copolymer and homopolymer coated electrodes using PARSTAT 4000A (AMETEK Scientific Instruments) with a conventional cell arrangement. The capacitance measurements for the M–S experiment were performed in 0.1 M Et_4NBF_4/ACN-DCM(3:1) solution. M–S experiments were done at a potential between −0.4 V and 1.5 V, and at a fixed frequency of 1 kHz with successive steps of 20 mV. Dissolved oxygen was removed by bubbling argon gas for 10 min before the M-S analysis.

Results and Discussion

Electrochemical polymerization and copolymerization of ProDOT and its derivative, and characterizations.—Figure 1 illustrates the steps of the electrocopolymerization process. Coupling reactions of ProDOT radical cations take place after the oxidation of the ProDOT monomer through electron transfer from the monomer to Si/graphene electrode followed by the dehydrogenation reaction (top). Further couplings of radical cations of oligomers formed, and the oxidation of these oligomers result in an oligomer-radical cation, which couples with the radical cation of an oligomer of ProDOT–EO–ester **2** (middle). The composition of the copolymer depends on the reactivity of each monomer (bottom).

The electrochemical polymerization of all homopolymers and copolymers was performed using cyclic voltammetry on Si/graphene substrate as a working electrode in 0.1 M Et_4NBF_4/ACN:DCM (3:1) electrolyte, and monomers (25 mM ProDOT-EO-Ester **2** and 25, 5, 1, 0.5 mM ProDOT **1**) or monomer mixtures with feed ratios of

Table I. Summary of PProDOT, P(ProDOT-EO-ester) and their copolymers.

Polymer		$\chi = \frac{[\text{ProDOT}]}{[\text{ProDOT}] + [\text{ProDOT} - \text{EO} - \text{ester}]}$
PProDOT		1
P(ProDOT-EO-ester)		0
P(ProDOT-co- ProDOT-EO-ester)		
$[\text{ProDOT}]_0/[\text{ ProDOT-EO-ester}]_0 = 1{:}1$	CP1-1	0.5
$[\text{ProDOT}]_0/[\text{ ProDOT-EO-ester}]_0 = 1{:}5$	CP1-5	0.16
$[\text{ProDOT}]_0/[\text{ ProDOT-EO-ester}]_0 = 1{:}25$	CP1-25	0.038
$[\text{ProDOT}]_0/[\text{ ProDOT-EO-ester}]_0 = 1{:}50$	CP1-50	0.020

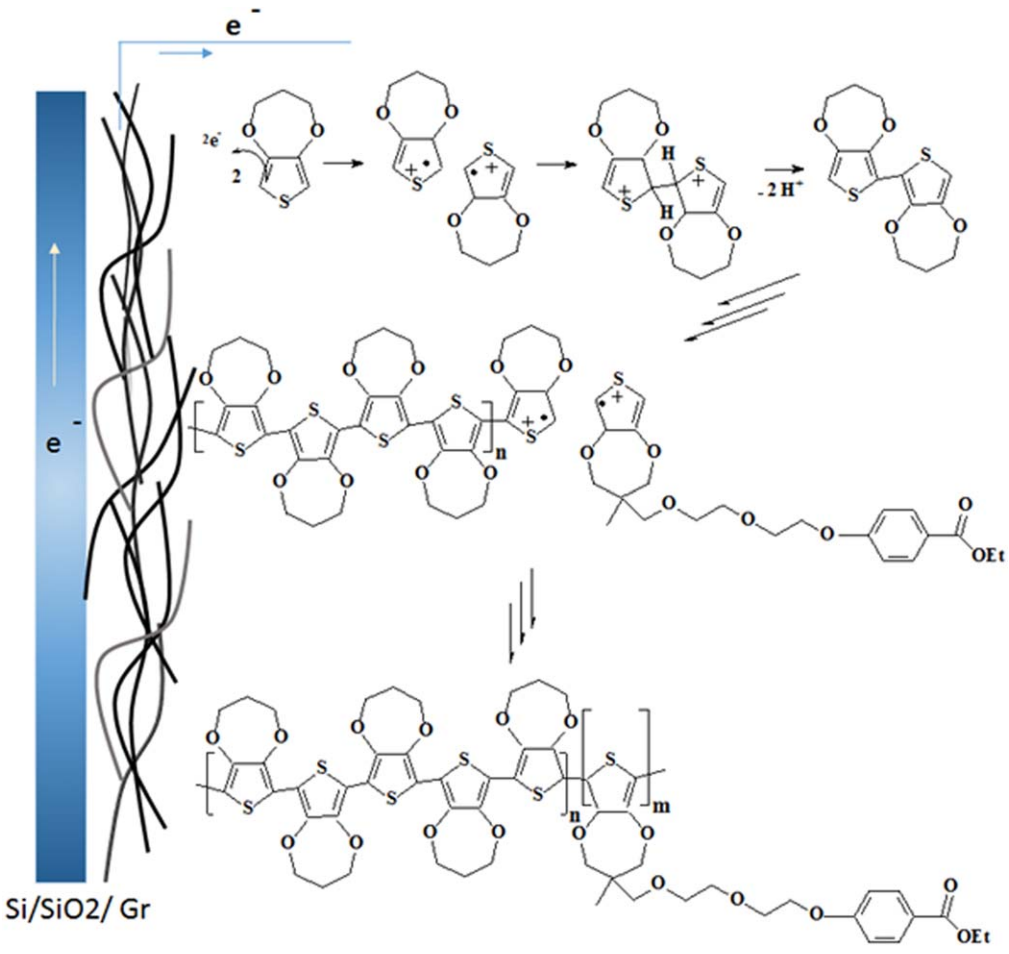

Figure 1. Schematics of electrochemical deposition and growth of copolymer on Si/graphene.

n_{ProDOT}:$n_{ProDOT\text{-}EO\text{-}Ester}$ of 1:1, 1:5, 1:25 and 1:50. During the anodic scan, the onset oxidation potentials (E_{onset}) of ProDOT, ProDOT-EO-ester, $[ProDOT]_0$:$[ProDOT\text{-}EO\text{-}ester]_0$ = 1:1, 1:5, 1:25 and 1:50 mole ratio were estimated from the first cycle of the electropolymerization and initiated at 1.45, 1.42, 1.40, 1.43, 1.45, and 1.44 V vs. Ag/AgCl, respectively. When compared to the ProDOT oxidation onset potential, P(ProDOT-EO-ester) shows the lowest value, whereas the copolymers have values in the mid-range (Fig. S2). Multistep cyclic voltammograms of 25, 5, 1, 0.5 mM ProDOT **1**, 25 mM ProDOT-EO-Ester **2** were applied to form the homopolymers and copolymers. In order to yield copolymer (ProDOT-co-ProDOT-EO-Ester), the feed ratio of ProDOT **1** to ProDOT-EO-Ester **2**: 1:1, 1:5, 1:25, 1:50 were used at the potential range from −0.5 to 1.6 V in 0.1 M Et_4NBF_4/ACN:DCM (3:1). An increase in the current density with each cycle was presented following peak potential values are obtained: E_{pa} (anodic peak) = 0.74 V, E_{pc} (cathodic peak) = 0.33 V for PProDOT **1**, E_{pa1} = 0.19 V, E_{pa2} = 0.46 V, E_{pc1} = 0.12 V, E_{pc2} = 0.36 V for ProDOT-EO-Ester **2**, E_{pa} = 0.65 V, E_{pc} = 0.39 V for CP1-1, E_{pa2} = 0.48 V, E_{pc1} = −0.46 V, E_{pc2} = 0.24 V for CP1-5, E_{pa1} = −0.02 V, E_{pa2} = 0.34 V, E_{pc1} = −0.24 V, E_{pc2} = 0.17 V for CP1-25, E_{pa1} = 0.15 V, E_{pa2} = 0.40 V, E_{pc1} = −0.15 V, E_{pc2} = 0.23 V for CP1-50, at the 10th cycle resulted in conducting homopolymer and copolymer thin films on Si/graphene electrode at 50 mV/s scan rate, see Figs. 2a–2f and Table SI. Two redox couple were observed for electrogrowth process for ProDOT-EO-Ester indicating the characteristic cyclic voltammetric response of oligoether bearing thiophenes.[43,58,59] The shift of both anodic and cathodic redox peak potential of P(ProDOT-EO-Ester) toward less anodic potential, when compared to that of PProDOT during the electropolymerization, can be explained by oligoether segments which are potentially capable of interacting with metal cation of electrolyte solution. As reported previously, electropolymerization of ProDOT,[42] polythiophene,[60] and poly(3,4-ethylenedioxythiophene)[58] bearing an oligoether chain lead to the complexation of cations from

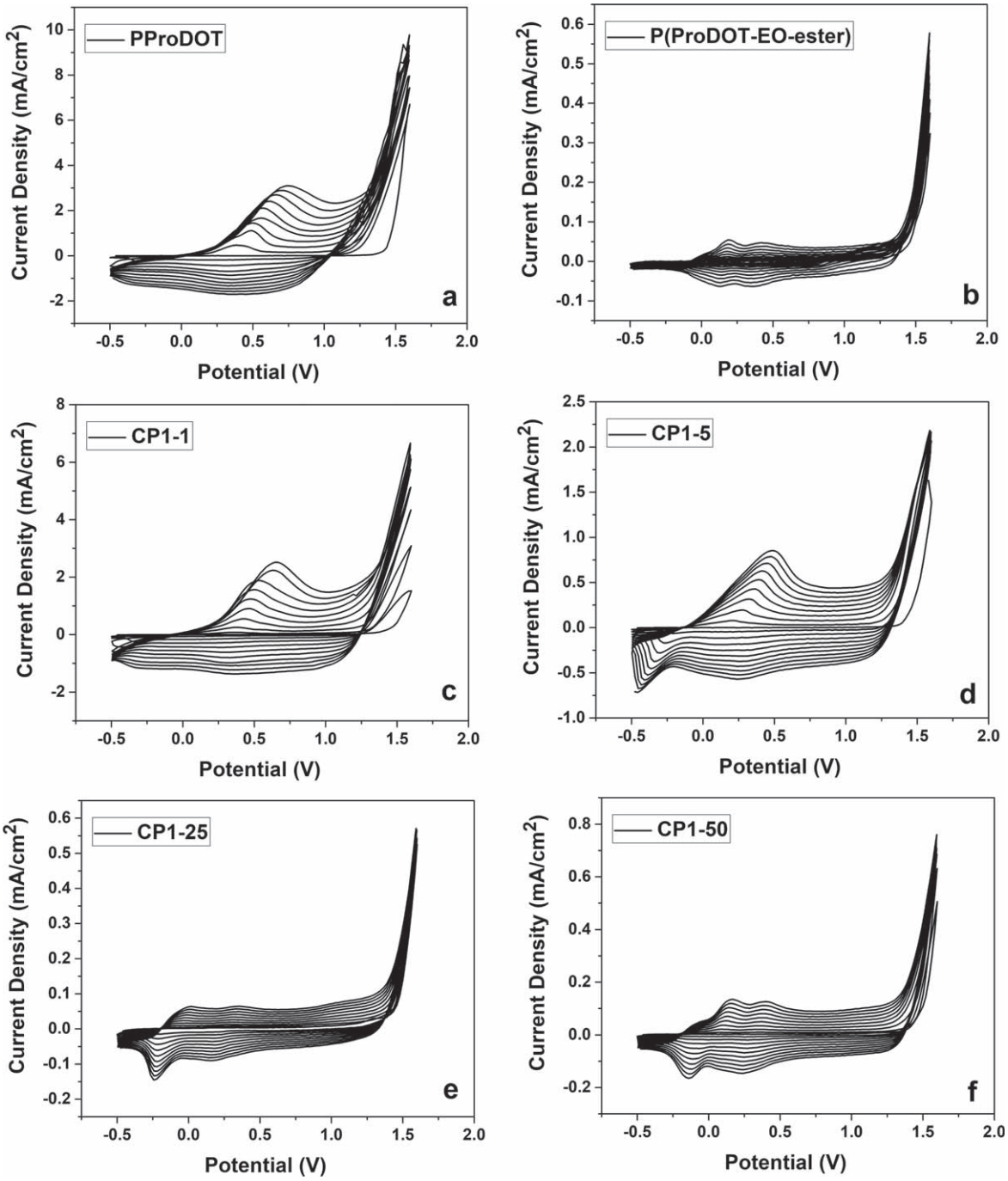

Figure 2. Cyclic voltammetry of (a) ProDOT (Q = 156.9 mC), $[ProDOT]_0$ = 25 mM, (b) P(ProDOT-EO-ester) (Q = 2.5 mC), $[ProDOT\text{-}EO\text{-}ester]_0$ = 25 mM, (c) $[ProDOT]_0/[ProDOT\text{-}EO\text{-}ester]_0$ = 1:1 (Q = 130 mC),(d) $[ProDOT]_0/[ProDOT\text{-}EO\text{-}ester]_0$ = 1:5 (Q = 62 mC),(e) $[ProDOT]_0/[ProDOT\text{-}EO\text{-}ester]_0$ = 1:25 (Q = 7.84 mC), and (f) $[ProDOT]_0/[ProDOT\text{-}EO\text{-}ester]_0$ = 1:50 (Q = 12.24 mC), on Si/graphene, potential range: −0.5–1.6 V, in 0.1 M Et_4NBF_4/ACN:DCM (3:1), 10 cycle, scan rate: 50 mVs^{-1}.

the electrolyte revealing a considerable influence on the peak potential related with the oxidation of the polymer and presenting good film quality. After increasing the mole fraction of ProDOT-EO-Ester **2**, the anodic and cathodic oxidation peaks for copolymers shift to negative potentials(Figs. 2c–2f) due to increasing complexation interaction of oligoether with cation of electrolyte.[61] It can be concluded that variations in redox potential due to the nature of the oligoether and ester chain significantly affect the electropolymerization process and possibly the structure of the polymer.

The linear increase in both anodic and cathodic peak currents of polymer coatings is illustrated in Fig. 3. The homopolymers and copolymers exhibit well-defined increasing peak current density with increasing sweep rate due to the oxidation/re-reduction processes of the polymer and copolymer films, and the redox behavior of the copolymer is completely different from homopolymers, which indicates the copolymer formation.

Electrochemical activity in comparison with both homopolymer and copolymer coated electrodes are given in Fig. 4 in a solution containing 0.1 M Et_4NBF_4/ACN:DCM (3:1) at a scan rate of 50 mVs^{-1}. As can be seen from Fig. 4a, PProDOT coated Si/graphene shows well-defined redox peaks.[48] However, there is no significant redox peak for P(ProDOT-EO-Ester) coated Si/graphene, where the shape of cyclic voltammogram (CV) is distorted from rectangular CV shape indicating an ohmic resistance of the electron

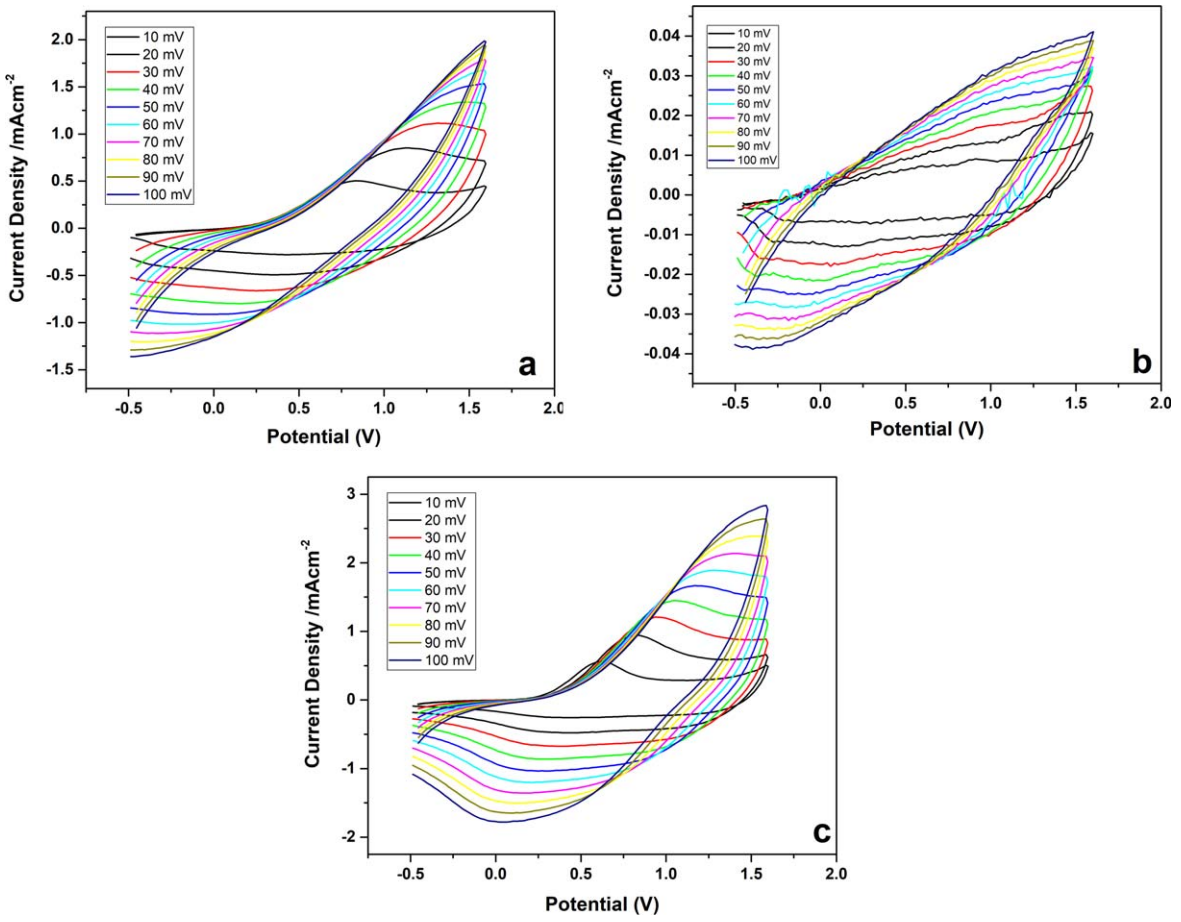

Figure 3. Cyclic voltammetry of (a) PProDOT, (b) P(ProDOT-EO-ester), (c) $[ProDOT]_0/[ProDOT\text{-}EO\text{-}ester]_0 = 1{:}1$, in monomer-free solution, in the potential range: −0.5–1.6 V, in 0.1 M Et_4NBF_4/ACN:DCM (3:1) at scan rates between 10 and 100 mVs^{-1}.

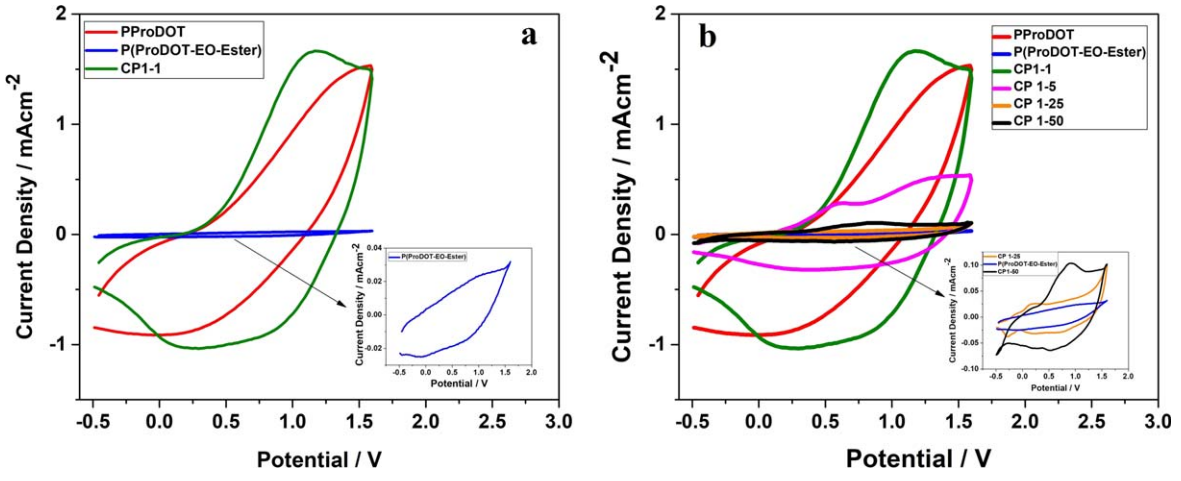

Figure 4. The CVs of (a) the PProDOT, P(ProDOT-EO-Ester), and CP1-1, inset in Fig. 4a shows the CV of P(ProDOT-EO-Ester) homopolymer, (b) all homopolymers and its copolymers (PProDOT, P(ProDOT-EO-Ester), CP1-1, CP1-5, CP1-25, and CP1-50) coated on the Si/Graphene electrode at the scan rate of 50 mVs^{-1} in 0.1 M Et_4NBF_4/ACN:DCM (3:1), and inset of Fig. 4b shows P(ProDOT-EO-Ester) homopolymer and copolymers of CP1-25 and CP1-50.

transfer and ionic movement in the polymer film similar to the previously reported CV of di-substituted PProDOT bearing ethyl and pure PEDOT (inset in Fig. 4a).[62,63] Moreover, the redox peaks for all copolymer coated Si/graphene electrodes are also well-defined in the CV response suggesting faster transport process with the cation of electrolyte and indicating enhanced pseudocapacitive characteristics by the copolymerization process.[64] In comparison to PProDOT and P(ProDOT-EO-Ester) coated electrodes, as the mole fraction of ProDOT reaches to 0.5, electrochemical response of the copolymer films increases, and thus, the best electrochemical activity is observed for CP1-1 coated Si/graphene electrode since it generates more current density compared to PProDOT and other copolymer films. This finding indicates that equal feed ratio of monomer leads to enhanced electrochemical properties can be comparable with previous works.[65–67] It has been corroborated from the impedance results that the highest electrochemical activity for the CP1-1 modified

Si/graphene electrode can be supported from a considerable decrease in the impedance (Z) value and superior charge-transfer resistance as compared with the other copolymer and homopolymer modified Si/graphene electrodes. By the increase of ProDOT in the copolymer composition, the higher dopant concentration is attained, suggesting an enhanced conductivity and agreeing well with the impedance and CV results. The difference in the conjugated structures between ProDOT and ProDOT-EO-ester due to the presence of the EO-ester group leads to a decrease in charge transfer resistance with the increasing mole fraction of ProDOT-EO-ester.

The scan rate dependencies of the homopolymer and copolymer coated electrodes were evaluated from the graphs of peak currents (i_p) vs. scan rate and i_p vs. the square root of the scan rate (Fig. 5). This allows deriving the correlation coefficients of the polymer-coated electrodes. According to these results, it can be concluded that the polymers exhibit a linear relationship between i_p and the square root of the scan rate with a high correlation coefficient (R_{an} = 0.9793–0.9997), indicating the diffusion-limited process.

The Randles–Sevcik equation at room temperature is described as[68]:

$$i_p = 268600\, n^{3/2} A C D^{1/2}\, \vartheta^{1/2} \qquad [1]$$

where i_p is the peak current density, n (1) the number of electrons transferred in the redox reaction, A is the electrode area (0.35 cm^2), D (cm^2 s^{-1}) is the diffusion coefficient estimated from the slope of the graph in Figs. 5c–5d, C is the diffusing species (mol cm^{-3}), and υ (V s^{-1}) is the scan rate. Since here n and C are the same for all samples, the slope of i_p vs $\vartheta^{1/2}$ gives the values of the diffusion-related parameters. For the anodic lines, these parameters are given in Table SII, where the slope increases to 0.321 for CP 1-1. Using the Randle–Sevick's equation and slope of I_p vs $\nu^{1/2}$ plot the diffusion coefficient of BF_4^- is estimated to be 6.43 × 10^{-11} cm^2 s^{-1} for PProDOT and 2.77 × 10^{-14} cm^2 s^{-1} for P(ProDOT-EO-Ester). In case of CP 1-1 coated Si/graphene, the diffusion coefficient of BF_4^- is estimated to be 1.43 × 10^{-10} cm^2 s^{-1}, which is about 2.23 times greater than PProDOT itself indicating an enhanced capacitive property. It can be concluded that the equal molar of the initial feed ratio increasingly facilitates the mass transport to a point, enabling a remarkable growth of the copolymer (CP1-1).

The average surface coverage, Γ^*, for both homopolymers and copolymers electrodeposited onto Si/graphene substrate can be calculated according to Eq. 2[69]:

$$\Gamma^* = Q/nFA \qquad [2]$$

where Γ^* is the average surface coverage in mol cm^{-2}, Q (C) is the total Faradaic charges occurred during the electropolymerization calculated from the half of integrated charge of cyclic voltammogram, n is the electron transfer number assumed as 2.25,[70] F is Faraday's constant (96485 C mol^{-1}), and A is the electrode area in cm^2.

The Γ^* values of the PProDOT, PProDOT-EO-Ester, and its copolymers (CP1-1, CP1-5, CP1-25, and CP1-50) are estimated to be 0.95, 0.02, 0.79, 0.38, 0.05 and 0.07 μmol cm^{-2} using Eq. 2, respectively. The lowest Γ^* is found for the PProDOT-EO-Ester as the preferred nucleation growth probably prevented more during the

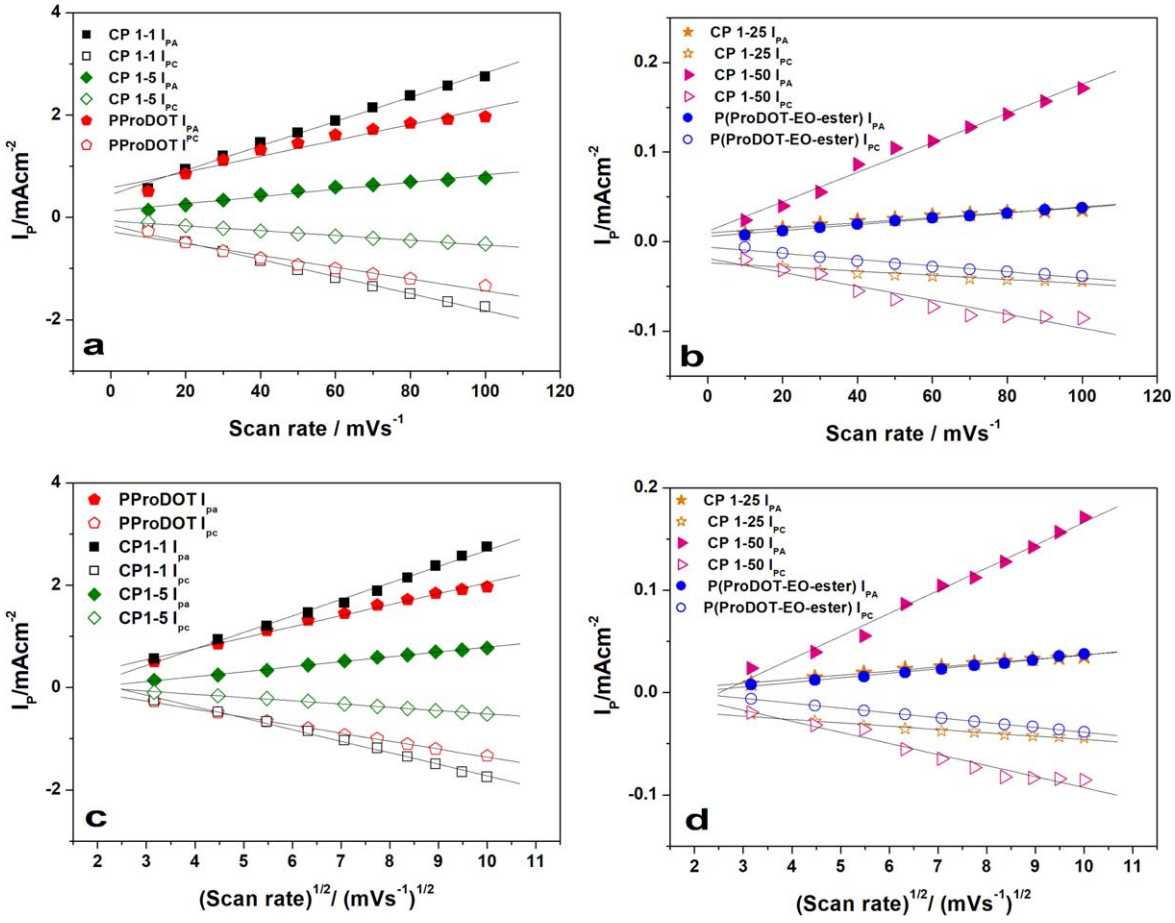

Figure 5. Scan rate vs current density and (a) and (b), square root of the scan rate vs current density plots (c) and (d) for PProDOT, P(ProDOT-EO-ester), CP1-1, CP1-5, CP1-25, and CP1-50.

polymerization compared to PProDOT due to the huge oligoether ester side group, which might induce sluggish rate of electropolymerization process. Moreover, within the copolymerization, as the mole fraction of ProDOT increased from 0.020 to 0.5, the average surface coverage increased from 0.07 μmol cm^{-2} for CP1-50 to 0.79 μmol cm^{-2} for CP1-1, where this rise indicates that the surface of Si/graphene electrode is more effectively modified with the equal molarity ProDOT and PProDOT-EO-ester.

The specific capacitance (C_{sp}) was calculated from CV measurements according to Eq. 3.

$$C_{sp} = \frac{\int idV}{2\nu\Delta VA} \quad [3]$$

where $\int idV$ is the integrated area under the CV curve, ν is the sweep rate (V s^{-1}), ΔV (V) is the potential window in CV measurements and A is the area in cm^2.

Fig. S3 shows the variation of C_{sp} with the scan rate. The calculated C_{sp} value was obtained at the scan rate from 10 to 100 mVs^{-1} . The C_{sp} values decrease with the increase of scan rates (see in Fig. S3). Since only the outer regions of the electrode can be accessed by the electrolyte ions at high scan rates, this decrease in C_{sp} can be attributed to incomplete diffusing of electrolyte ions to the electrode surface.[71] The C_{sp} of copolymer modified Si/Graphene electrode increases with increasing mole fraction of ProDOT. Among the copolymers, the highest C_{sp} is estimated as 19.46 mF cm^{-2} for the CP1-1 at a scan rate of 10 mV s^{-1} indicating an optimum capacitive property when reaching to the equal feed ratio of ProDOT and ProDOT-EO-ester monomers.[65] Moreover, the high capacitive property for CP1-1 becomes more pronounced with increasing scan rate in comparison with those of homopolymers and its copolymers. These results are higher than the reported areal capacitance value for other nanostructured electrode systems such as PEDOT:PSS/AgNFs/NOA/PET (3.64 mF cm^{-2} at 10 mV s^{-1}),[72] PANI/NPG (6.54 mF cm^{-2} at 10 mV s^{-1}),[73] PANI/AuNW (11.76 mF cm^{-2} at 10 mV s^{-1}),[74] and on the other hand, the areal capacitance values reported here are comparable to that of ZnONRs@CuS@PEDOT@MnO2/ITO (19.85 mF cm^{-2} at 5 mV s^{-1}).[75]

The FTIR-ATR transmittance spectra of PProDOT, P(ProDOT-EO-ester), CP1-1, CP1-5, CP1-25 and CP 1-50 are shown in Figs. 6a–6c confirmed the presence of both ProDOT and ProDOT-EO-ester units in the copolymer composition. As shown in Fig. 6a, the absorption band characteristics of the PProDOT homopolymers appear at 1401, 1310, 1181, 1046, 912, 817, and 692 , respectively. The bands appeared at 1401 cm^{-1} and 1310 cm^{-1} can be attributed to the C=C stretching in polythiophene. The bands at about 1181 and 1046 cm^{-1} correspond to the C–O–C bond stretching in the alkylenedioxy group. The C–S–C bonds in the thiophene ring is observed at 912, 817, and 692 cm^{-1}.[76] The bands at 608 and 430 cm^{-1} indicate the formation of the polaronic charges in thiophene.[77] P(ProDOT-EO-ester) also shows characteristic infrared bands: the aromatic C=C stretching vibration appearing at 1485 cm^{-1} is characteristic for monomeric thiophene in the polythiophene indicating successful polymerization. The C–O–C bond stretching for P(ProDOT-EO-ester) appeared at 1152 and 1052 cm^{-1} is overlapped due to the same bond stretching characteristic of both alkylenedioxy group and oligoether side chain.[78] The C=O stretching band appeared at 1630 cm^{-1} (Fig. 6a). The weak peak at 2974 cm^{-1}can be attributed to the CH_3 stretching of the methyl units.[79] Besides, all weak and broad peaks appearing around 3600 cm^{-1} can be attributed to the C–OH vibration due to the presence of the monolayer graphene structure on the silicon substrate.[80] All copolymers show transmittance bands related to both ProDOT and ProDOT-EO-ester. Moreover, as shown in Figs. 6b–6c, when comparing copolymers of different ProDOT:ProDOT-EO-ester ratios, the C–O–C stretching band (around 1152 and 1052 cm^{-1}) due to both alkylenedioxy group in ProDOT backbone and oligoether side chain of ProDOT-EO-ester become more intense with increasing amount of ProDOT-EO-ester monomer confirming success in copolymerization process.

The Raman spectra of PProDOT, P(ProDOT-EO-ester), CP1-1, CP1-5, CP 1-25 and CP1-50 are shown in Fig. 7. As presented in Fig. 7, PProDOT exhibits bands at 1479 and 1401 cm^{-1}. These bands are related to the thiophene groups in PProDOT and correspond to asymmetric C_α=C_β and symmetric C_α=C_β stretching. The bands at 1276 and 1218 cm^{-1} are attributed to C_β–C_β stretching and C_α–C_α inter-ring stretching of the thiophene ring, respectively. The C–O–C deformation is observed at 1089 cm^{-1}.[81] The characteristic bands of P(ProDOT-EO-ester) are similar to that of PProDOT. The bands at 1510 and 1388 cm^{-1} are attributed to asymmetric C_α=C_β and symmetric C_α=C_β stretching. C_β–C_β stretching and C_α–C_α inter-ring stretching of the thiophene ring is observed at 1268 and 1213 cm^{-1}, respectively. The band at 1089 cm^{-1} is assigned to the C–O–C deformation. All copolymers show similar characteristic Raman bands as those of PProDOT and P(ProDOT-EO-ester) due to the same repetitive ProDOT structure of the polymer backbone.

Figure 8 shows the XRD patterns of PProDOT, P(ProDOT-EO-ester) and the copolymers. For each sample, the Si[82] substrate has a broad peak at 15.8°. The sharp XRD patterns at 2Θ = 26.9° for PProDOT, 26.1°for CP1-1 and 26.9° for CP1-5 are attributed to the interchain planar ring stacking distance with plane (020) reflection.[82] The sharp XRD patterns at 2Θ = 29.2° for PProDOT and 18.8° 19.77°,, 29.3°, 32.5° for CP1-1 are observed indicating a small degree of crystallinity coming from the PProDOT.[83,84] In contrast, P(ProDOT-EO-ester), CP1-5, CP1-25, and CP1-50 have an amorphous structure just like some other polythiophene derivatives.[85]

Optical microscope images of the electrocoating are displayed in Fig. S4. The clearly visible crystalline structure of PProDOT becomes less pronounced by copolymerization with an increasing amount of ProDOT-EO-Ester **2**. The PProDOT-EO-Ester does not show any crystallinity (see the XRD results). This change could also be the reason for the photochromic effect which varies with the composition.

The morphological features of the electro-polymerized/copolymerized films deposited on Si/graphene substrate were examined by field emission gun scanning electron microscopy (FEGSEM). Figures 9a–9f depict the surface morphologies of the homo-polymer and copolymer coated Si/graphene substrate. The PProDOT film displays polymeric grains distributed uniformly over the Si/graphene substrate with porous structures (see high magnification SEM image in Fig. 9a inset). The P(ProDOT-EO-ester) film presents aggregates of non-uniform sized swelled structures on the substrate (see high magnification SEM image in Fig. 9b inset). CP1-1 and CP 1-5 show similar morphology like PProDOT, but grain sizes of polymeric structures are smaller than that of PProDOT (Figs. 9c and 9d). Moreover, the grain sizes of the polymeric structures decrease with increasing amount of ProDOT-EO-ester **2**, presenting quite smooth and dense morphology in case of CP 1-25 and CP1-50(Figs. 9e and 9f, respectively). These different structures originate from the growth mechanism of the copolymer film and different reactivity ratio of monomers. This fact also reveals that the copolymer morphology is influenced by the initial feed ratios of the monomers.

The EDX elemental mapping analysis (Figs. S5a–S5f) suggests that ProDOT **1** and ProDOT-EO-ester **2** units are uniformly dispersed on the copolymer films, as evidenced by the homogeneous distribution of C, O, and S. The uniform distribution of C, O, and S at different monomer feed ratio also suggests that the PProDOT and the P(ProDOT-EO-ester) are randomly ordered in the copolymer chains without the formation of block copolymers. This is understandable because the copolymer was deposited at the same potential as the homopolymers, and hence, the polymerization of both ProDOT **1** and ProDOT-EO-ester **2** takes place simultaneously. When the mole ratio (n_{ProDOT}:$n_{ProDOT\text{-}EO\text{-}Ester}$) 1:25 and 1:50 is compared to the mole ratio 1:1 and 1:5, the copolymer is expected to have more C and O distribution due to the inclusion of EO-ester group as a substituent group of the ProDOT unit. As a result, its

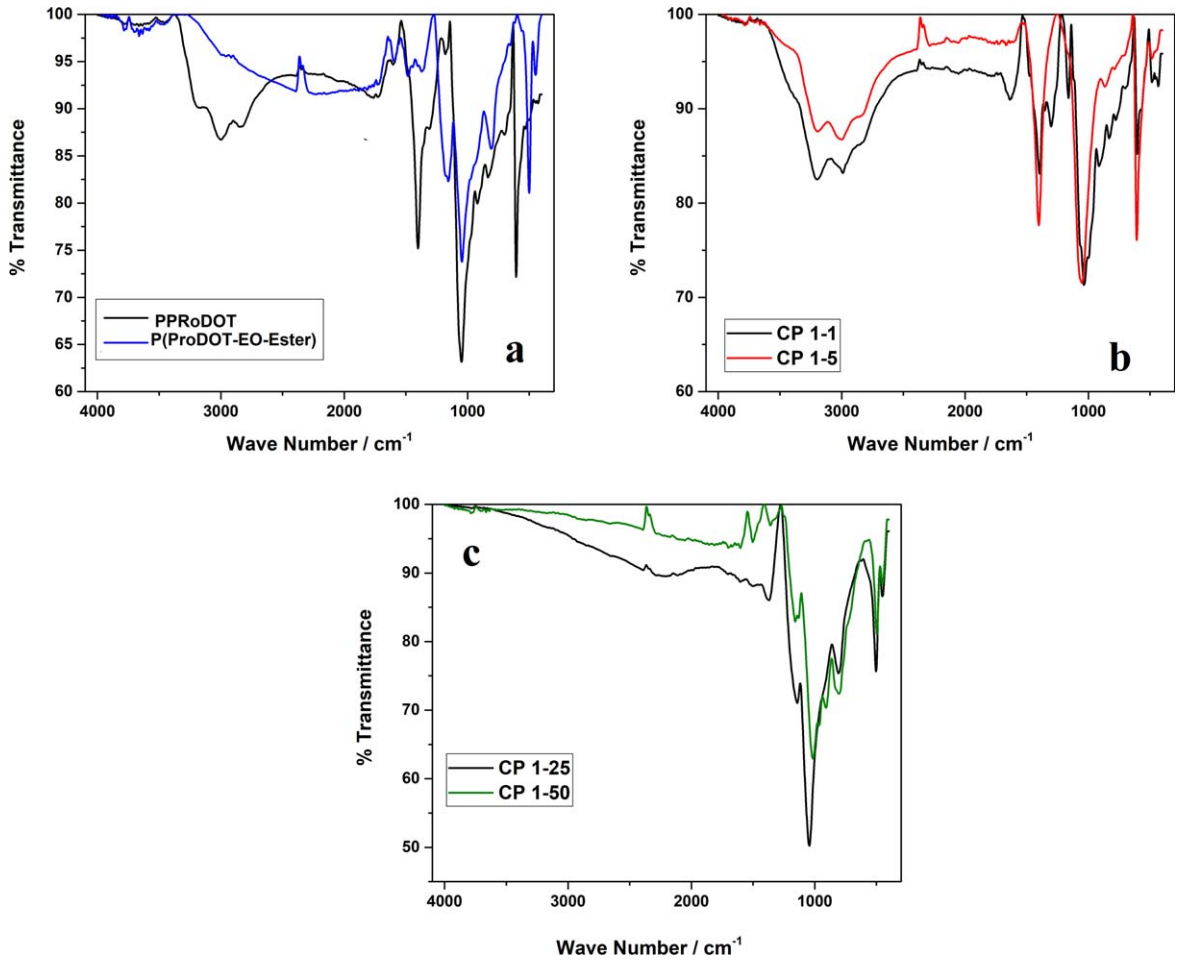

Figure 6. FTIR-ATR spectra of (a) PProDOT and P(ProDOT-EO-ester), (b) CP1-1 and CP1-5, and (c) CP 1-25 and CP1-50.

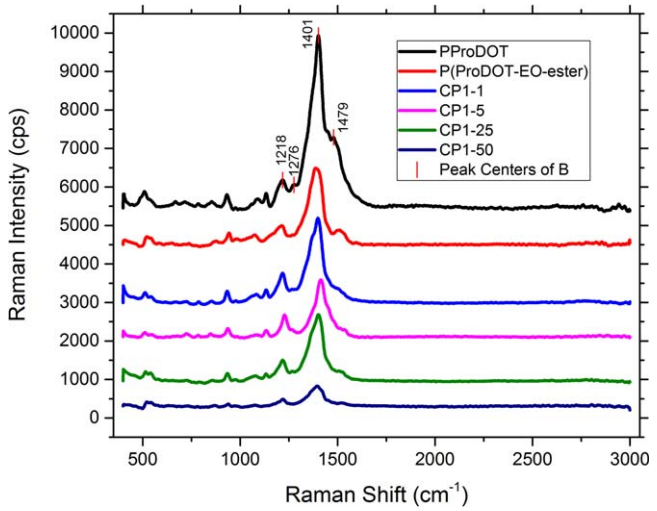

Figure 7. Raman spectra of PProDOT, P(ProDOT-EO-ester), CP1-1, CP1-5, CP 1-25, and CP1-50.

charge carrier mobility and polaron state, as well as its electrochemical behavior, probably show more substantial alteration.

Three dimensional AFM images for the PProDOT, P(ProDOT-EO-ester) and the copolymer films (CP1-1, CP1-5, CP 1-25 and CP1-50) coated on the Si/graphene are shown in Figs. 10a–10d. Electrochemical deposition leads to the formation of a conducting film consisting of aggregates of a few micrometers size, which is in agreement with previous results.[50,86] The root-mean-square (RMS) surface roughness of PProDOT, P(ProDOT-EO-ester), CP1-1, CP1-5, CP1-25, and CP1-50 were calculated from the 5×5 μm^2 scan area as 70.84 nm, 7.12 nm, 65.16 nm, 48.59 nm, 35.88 nm, 14.51 nm, respectively. These results suggest that with increasing molar ratio of ProDOT-EO-ester **2**, denser, uniform and smooth surfaces are obtained. These results can be compared with the data in the literature that the chemical copolymerization of aniline and o-bromoaniline upon increasing ratio of o-bromoaniline to aniline in the feed, and copolymerization with the increasing composition of o-bromoaniline result in a decrease in the yield of copolymers due to steric hindrance of bromine group with more smooth and uniform surface.[87] Therefore, the reason for smooth and uniform surface with increasing amount of ProDOT-EO-Ester can be attributed to a decrease in the yield of copolymers due to steric hindrance as the huge size of the EO-ester probably decreases the rate of copolymerization process in spite of the high concentration of ProDOT-EO-Ester monomer. In addition, it was stated in a previous study that, polythiophene bearing oligoether chain[88] showed a smoother and more compact morphology compared to fibrillary morphology of poly(3-hexylthiophene). Furthermore, the degree of average roughness poly(α-tetrathiophene) prepared by electrochemical polymerization increased as the polymer film yield increased.[89]

Electrochemical impedance spectroscopy and equivalent circuit modeling.—The characterization of the electrical properties of the polymer films with the change of composition of ProDOT and P (ProDOT-EO-ester) on the capacitance and resistance of copolymer films displayed remarkable differences in impedance values. This difference is apparent from the shapes of the impedance spectra

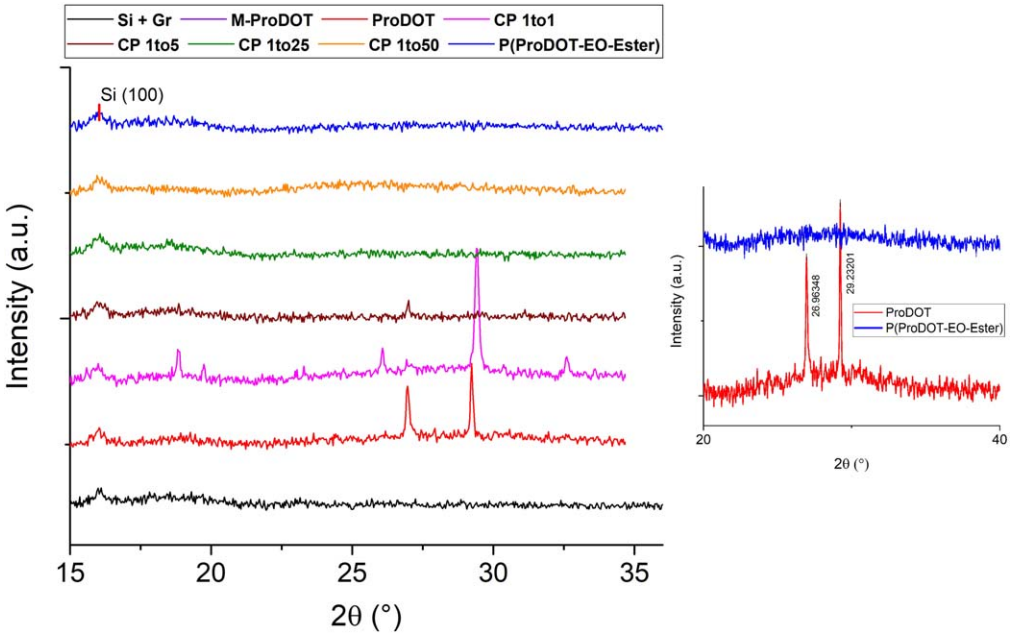

Figure 8. X-ray diffraction (XRD) patterns of PProDOT, P(ProDOT-EO-ester) and its copolymers. The inset figure shows that the particular ProDOT peaks are indexed in comparison to its ester derivative.

given in Figs. 11a–11d which show the Nyquist diagrams of all considered polymer-coated Si/graphene electrodes. A well-defined semicircle at high frequency is observed for all P(ProDOT-EO-ester), CP1-1, CP1-5, CP1-25, and CP1-50, except for PProDOT, indicating the charge transfer process between the Si/graphene/polymer/solution interfaces. The semicircle is followed by a vertical line for CP1-25 and CP1-50 coated Si/Graphene electrodes at the medium to low-frequency region revealing the interfacial double-layer capacitance,[90] whereas a linear line with a slope of 45° at the frequency nearby 158.5 mHz for P(ProDOT-EO-ester) and 3.16 Hz for CP1-5 coated Si/graphene electrodes indicates the Warburg diffusion behavior due to migration and diffusion of ions through the polymer film.[91] PProDOT shows a slight inductive behavior within a decrease in impedance value at the both imaginary and real part after the frequency of 31.2 mHz (see Fig. 11a).CP1-1 also shows an inductive behavior by decreasing in impedance value at the real part and with increasing in impedance value at the imaginary part after the frequency of 2.512 Hz (see Fig. 11c). This behavior is probably attributed to the surface feature of those of polymer coated Si/graphene electrodes or diffusion of electrolyte ions.[92,93] An inductive effect of the electro-synthesized polyaniline/reduced graphene oxide nanocomposite was reported, which was attributed to the conversion of benzoquinone to hydroquinone in polyaniline.[94] Kathuroju and Nagaraju reported an inductive behavior for electropolymerized polypyrrole microstructures where inductive characteristic was linked to the coral shape structures.[92] Charron et al. reported an inductive loop for the electropolymerized thiophene derivative (diphenyldithieno [3,2-b;20,30-d]thiophene) in a specific bis(trifluoromethylsulfonyl)amine lithium (LiTFSI)/ACN electrolyte, which was related to the diffusion of two ionic species (Li^+ and $TFSI^-$) in opposite directions during the polarization of the conducting polymer film.[93]

As can be seen in Fig. 11d, all copolymer coated Si/graphene electrodes exhibit lower semicircle diameter compared to both ProDOT and P(ProDOT-EO-ester) homopolymers. Therefore, it can be concluded that the copolymerization facilitates the charge transfer process between the polymer films and the solution interface leading to polymer films of higher conductivity.

The capacitance value of polymer coated Si/graphene electrodes increases at low frequencies due to the movement of more ions, leading to a decrease in the bulk resistance of the electrode. The low-frequency capacitance (C_{LF}) was calculated from the imaginary part of the impedance (Z_{im}) diagram at the lowest frequency of 0.01 Hz using the following Eq. 4:

$$C_{LF} = \frac{1}{2\pi f Z_{im}} \quad [4]$$

The calculated capacitance values are listed in Table SIII. The highest low-frequency capacitance (C_{LF} = 290.8 μFcm^{-2}) was calculated for CP 1-1 at a frequency of 0.01 Hz, which can be attributed to the porous surface structures, high surface roughness and high conductivity of CP1-1. This finding indicates that the equal molar of initial feed ratio is the best threshold for copolymer composition, where the close correlation between the DC (CV) and AC (EIS) mode measurements indicates the seamless match of both experimental results.

The Bode-phase plots of the homopolymer and copolymer coated Si/graphene electrodes are depicted in Fig. S6. The hump maximum appeared at the medium frequency domain for homopolymers decreases and shifts to higher frequencies for copolymers with the increasing mole fraction of ProDOT-EO-ester **2**. The semi-hump for copolymer with the increasing mole fraction of ProDOT-EO-ester appears at the low-frequency domain with increasing phase angle close to 90° because the linear region tilts towards the imaginary axis in the low frequency region (see Figs. 11c–11d), and this indicates good capacitive behavior as the angle ϕ reaches to ~90.[95] The maximum phase angles are 83° at 224 Hz, 84° at 326 Hz, 72.5° at 1985 Hz, 78.2° at 994 Hz, 82° at 10 mHz and 81.1° at 10 mHz for PProDOT, P(ProDOT-EO-ester), CP1-1, CP1-5, CP1-25, and CP1-50, respectively.

EIS provides information about the interfaces of an electrode while presenting the various time constants associated with the electrochemical processes. Figure 12 shows the Bode magnitude graphs. The highest magnitude of impedance (IZI) is attained for PProDOT coated Si/graphene electrode, whereas the lowest IZI is attained for CP1-1 coated Si/graphene electrode. Moreover, all copolymer coated Si/graphene electrodes present a low value of IZI compared to homopolymer coated Si/graphene electrodes indicating an enhanced conductivity with the copolymerization process.

It is possible to find a direct correlation between the response of a measured and calculated impedance values by a simple model of $R_s(Q1(R_{CT}Q2))$ as an equivalent circuit (inset in Fig. 12). The validity of fitting to the corresponding circuits is first assessed by the

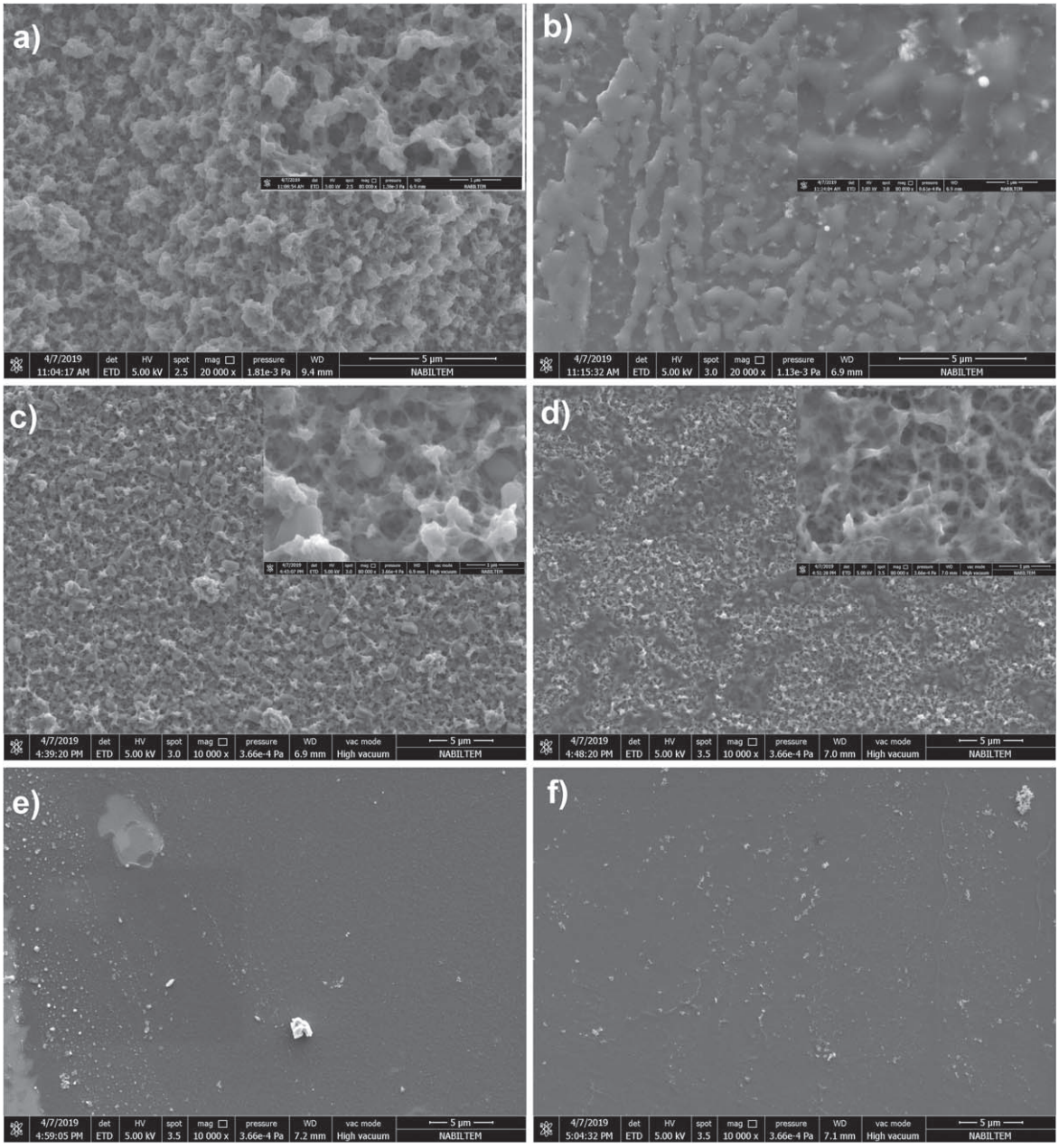

Figure 9. FEGSEM images of (a) PProDOT, (b) P(ProDOT-EO-ester), (c) CP1-1, (d) CP1-5, (e) CP 1-25, and (f) CP1-50, each scale bar is 5 μm. The insets show high magnification images of the corresponding films, and inset scale bar is 1 μm.

chi-squared (χ^2), where the error of each element is less than 7%. Measured and calculated impedance for all the polymer-coated Si/graphene electrodes are shown in Fig. 12 confirming the validity of the proposed circuit due to the well-fit of the measured impedance data in the whole frequency range. The first resistance corresponds to the solution resistance which is the sum of the electrolyte resistance and the polymer electronic resistance. Constant phase element (CPE) was introduced to the equivalent circuit related to the inhomogeneity, roughness or fractional geometry of the electrode and electrode porosity.[46] Since the semicircle results from the parallel combination of resistance and capacitance, the parallel connected *RQ* elements (R_{CT} and $Q1$) describes the electrolyte/polymer interface which are the double layer capacitance and charge-transfer resistance, respectively.[96] $Q2$, which is a series connection with R_{CT} element, is ascribed for the polymer film capacitance. The calculated data are shown in Table II.

The charge transfer resistance significantly decreases with the coating of Si/graphene by CP1-1 that can be assigned to the high conductivity of CP1-1. The R_{CT} of CP1-1 coated Si/graphene has nearly 51 and 24 times lower value compared to those of PProDOT and P(ProDOT-EO-ester) homopolymers coated electrodes, respectively, confirming that the copolymerization improves the electron conduction.

The presence of a constant phase element instead of a capacitance reveals the frequency dispersion of the electric double layer commencing from the surface porosity or inhomogeneity of the surface of the electrode materials. The impedance of the CPE can be represented as;

$$Z_{CPE} = \frac{1}{Y_0(j\omega)^n} \quad [5]$$

Here, Y_0 is the pre-factor of CPE, and n is the CPE-exponent, which is related to the frequency in the range of 0 to 1 , where 0 and 1 correspond to the resistor and capacitor, respectively. As can be seen in Table I, the capacitance for CP1-1 film shows remarkable differences compared to all homopolymers and copolymers coated

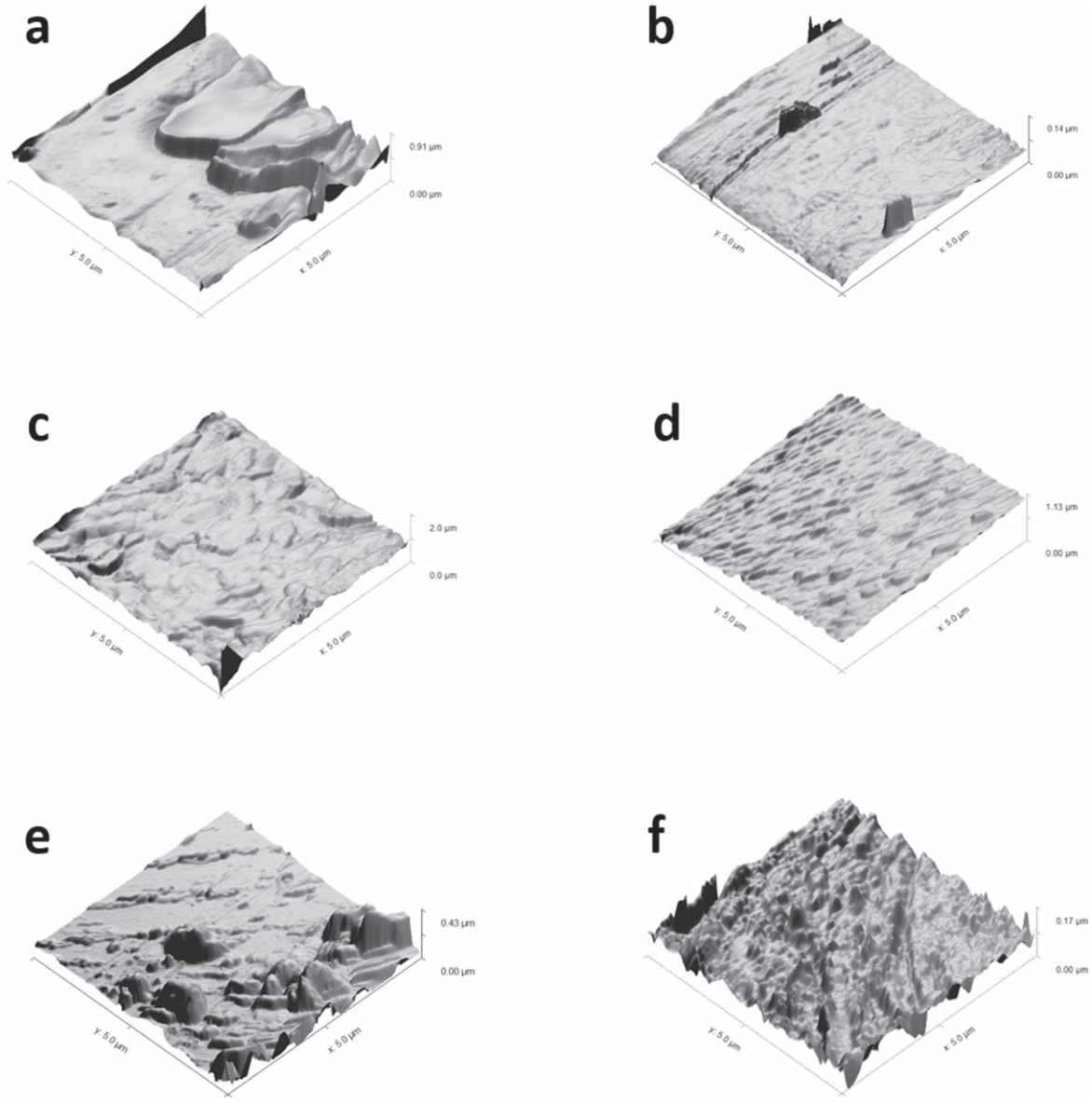

Figure 10. AFM images of (a) PProDOT, (b) P(ProDOT-EO-ester), (c) CP1-1, (d) CP1-5, (e) CP 1-25, and (f) CP1-50.

Si/graphene electrodes corroborating the equal molar of initial feed ratio is the best threshold for copolymerization, and capacitance of other copolymer films generally decrease with the increasing mole fraction of ProDOT-EO-ester **2**.

Interfacial properties of polymer modified Si/Graphene electrode/electrolyte.—In order to analyze the dependence of the semiconducting properties on the compositions of the copolymers, the impedance measurements were performed at various applied biases for defining a Mott-Schottky type of analysis. The applied bias potential was recorded in a range between −0.5 V/(Ag/AgCl) and +1.5 V/(Ag/AgCl), where all the polymer films showed redox activity at the explored potential range in 0.1 M Et_4NBF_4/ACN:DCM(3:1) electrolyte at a fixed frequency of 1 kHz. The interfacial capacitance was calculated from the imaginary part of the impedance diagram.[97] In depletion conditions, the interfacial capacitance is equal to the space region capacitance (C_{SC}). Thus, a Mott-Schottky plot can be constructed by plotting the inverse of squared C_{SC} ($1/C_{SC}^2$) against the applied bias potential (Fig. 13).

The Mott-Schottky equation can be expressed for p-type semiconductor as[98]:

$$\frac{1}{C_{SC}^2}A^2 = \left(\frac{2}{\varepsilon\varepsilon_p e N_D}\right)\left(-E + E_{FB} - \frac{k_B T}{e}\right) \quad [6]$$

Here, C_{SC} is the space-charge capacitance, A is the area, N_D is the donor density, E is the applied voltage, E_{FB} is the flat band potential, k_B is Boltzmann's constant, T is the absolute temperature, e is the electronic charge, ε is the vacuum permittivity, and ε_p is the relative permittivity of polymer films assumed to be 3.5.[99]

Mott-Schottky plots for PProDOT, P(ProDOT-EO-ester), CP1-1, and CP1-5 are given in Figs. 13a–13d. For the bias potential from −0.5 to −0.3 V, the value of the inversed square capacitance increases for PProDOT and CP1-1. This behavior can be ascribed to the formation of an inversion layer leading to an apparent n-type conductivity.[82] A linear region up to 0.6 V for PProDOT, CP1-1, and CP1-5 describes semiconducting behavior within a considerable decrease of inversed squared capacitance, where no redox peak

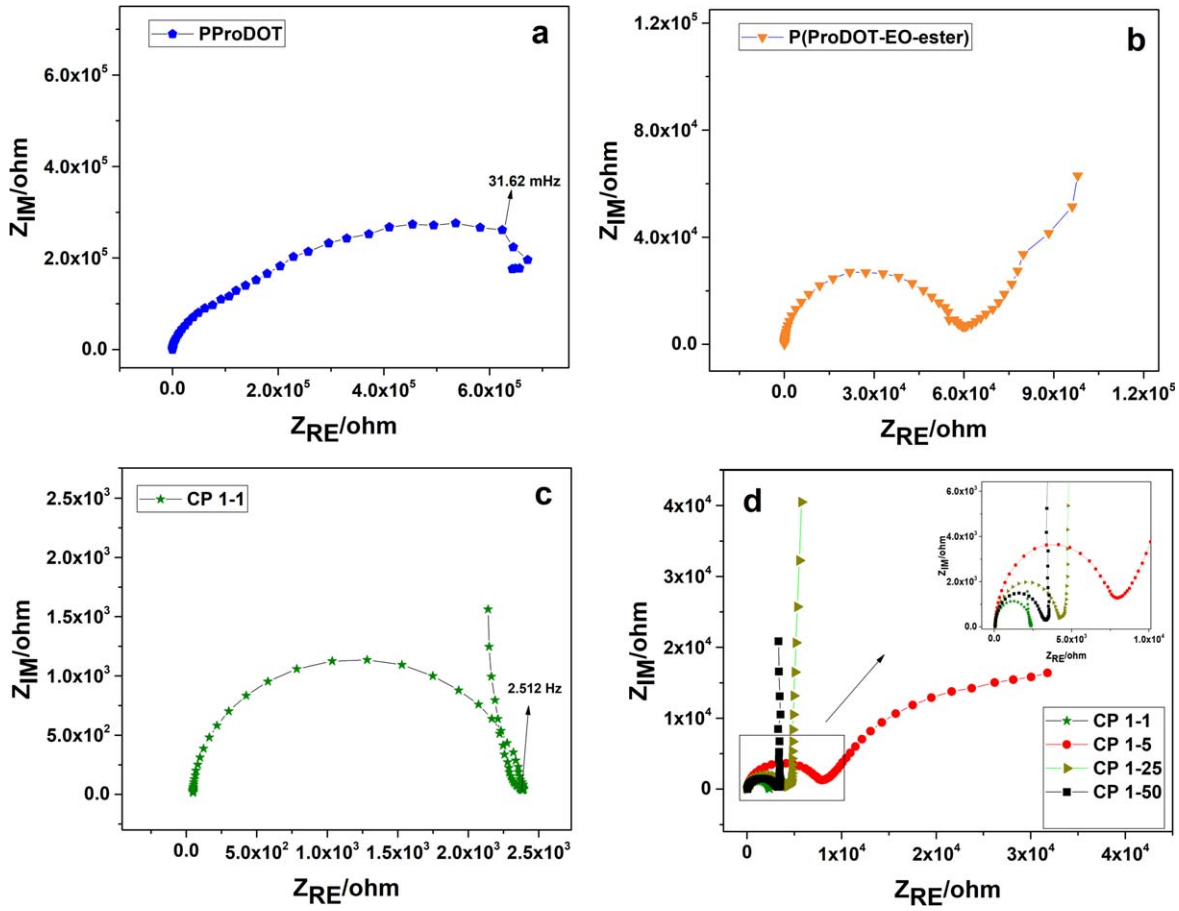

Figure 11. Nyquist diagrams for (a) PProDOT (b) P(ProDOT-EO-ester), (c) CP1-1, and (d) CP1-1, CP1-5, CP1-25 and CP1-50 for comparison. Frequency range: 10 mHz–100 kHz, 10 mV DC amplitude at open circuit potential conditions.

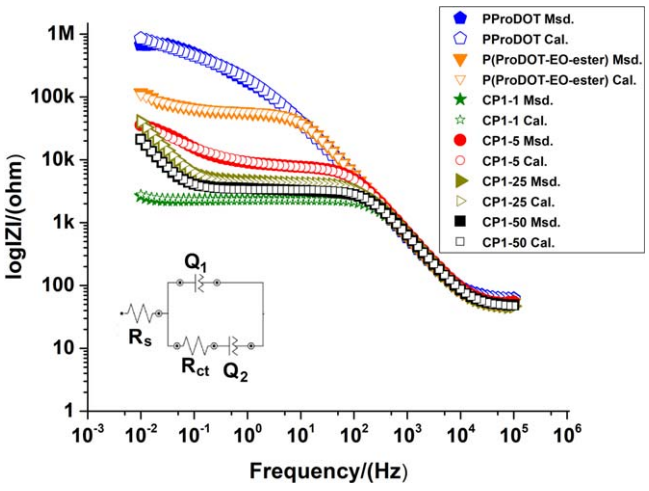

Figure 12. Measured and calculated impedance values of the Bode magnitude diagrams of PProDOT, P(ProDOT-EO-ester), CP1-1, CP1-5, CP1-25 and CP1-50. The inset shows proposed equivalent circuit model (ECM) adopted for all polymer samples.

could be observed from CV measurement for these coated polymer films. However, as can be seen in Fig. 13b, a considerable decrease or increase in inversed squared capacitance did not appear for P (ProDOT-EO-ester) coated Si/Graphene electrode indicating its poor semiconducting behavior. The E_{FB} and N_D values were estimated from the linear part of the Mott-Schottky plots indicating the formation of a space charge layer at the semiconductor side. The Mott-Schottky parameters for PProDOT, CP1-1, and CP1-5 are summarized in Table III.

For the PProDOT coated Si/Graphene (see Fig. 13a), the linear parts in the potential range 0.2–0.6 V indicate p-type semiconducting behavior with a negative slope. The N_D and E_{FB} values for PProDOT are calculated as 3.45×10^{19} cm^{-3} and 2.15 V, respectively. With the copolymerization, semiconducting properties are observed, as can be seen from Figs. 13c and 13d, due to the linearity by a decrease in the value of the inversed square capacitance. For the equal molar of initial feed ratio (CP1-1), the N_D was estimated as 2.25×10^{19} cm^{-3} and E_{FB} was 1.40 V. Moreover, N_D was estimated as 9.70×10^{18} cm^{-3} and E_{FB} was 0.62 V for CP1-5 which is shifted to low positive value with the increasing mole fraction of ProDOT-EO-ester **2**. Moreover, as the mole fraction of ProDOT **1** increases in the copolymer composition, the higher dopant concentration is attained, suggesting an enhanced conductivity that agrees well with the impedance and CV results.

The oxygen content (%) vs average surface coverage (Γ^*) values calculated from the CV measurements are plotted in Fig. S7a. At low obtained Γ^* (corresponding to a low [ProDOT **1**]/([ProDOT **1**] +[ProDOT-EO-Ester **2**] ratio and low charge), higher O contents are observed due to the lower oxidation potential of ProDOT EO Ester **2** monomer compared to ProDOT **1**. The constant phase element (Q_2), which corresponds to the capacitance of polymer films, and the slope of I_p vs. the square root of the scan rate (in monomer-free solution) for the [ProDOT **1**]/([ProDOT **1**]+[ProDOT-EO-Ester **2**]) giving maximum, while charge transfer resistance giving a minimum at 1:1 mole ratio of ProDOT **1**/ProDOT EO Ester **2** indicate that CP1-1 is a high conducting and capacitive copolymer film (Fig. S7b). The charge (Q) (from electrogrowth) is obtained from the CVs and the anodic peak current density is obtained at a scan rate of 50 mV s^{-1}

Table II. Equivalent circuit model parameters for PProDOT, P(ProDOT-EO-ester), CP1-1, CP1-5, CP 1-25, (f) CP1-50.

Si/Graphene/Polymer	R_s/ohm	Q_1/Y_0/Ssec^n.cm^{-2}	n_1	R_{CT}/kohmcm^2	$Q2/Y_0$/Ssec^n.cm^{-2}	n_2	$\chi 2$
PProDOT	57.9	1.43×10^{-6}	0.93	41.30	8.55×10^{-6}	0.30	91.8×10^{-4}
P(ProDOT-EO-ester)	49.5	9.47×10^{-7}	0.97	19.92	2.47×10^{-4}	0.62	22.3×10^{-4}
CP1-1	48.6	8.39×10^{-7}	0.98	0.80	2.89×10^{-2}	1	14.0×10^{-4}
CP1-5	50.2	8.08×10^{-7}	0.97	2.50	3.63×10^{-4}	0.52	43.0×10^{-4}
CP1-25	44.3	9.94×10^{-7}	0.96	1.52	1.02×10^{-3}	0.96	12.5×10^{-4}
CP1-50	46.4	1.01×10^{-6}	0.96	1.16	2.07×10^{-3}	0.98	17.9×10^{-4}

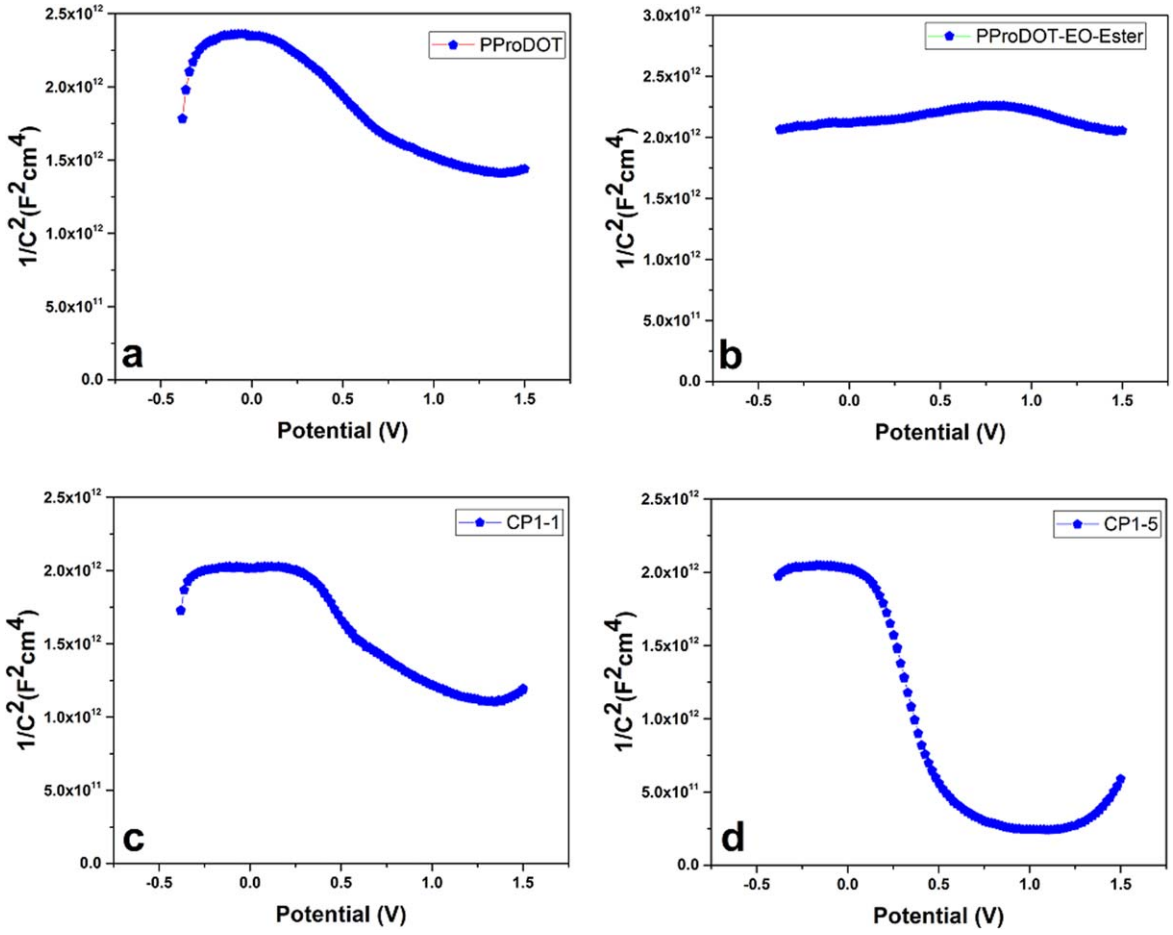

Figure 13. Mott-Schottky plots for PProDOT, P(ProDOT-EO-ester), CP1-1, (d) CP1-5.

Table III. Mott-Schottky parameters for PProDOT, CP1-1, CP1-5 coated electrodes.

Electrode	N_D cm^{-3}	E_{FB}/V	Conductivity Type
PProDOT	3.45×10^{19}	2.15	*p*
CP1-1	2.25×10^{19}	1.40	*p*
CP1-5	9.70×10^{18}	0.62	*p*

for polymer-coated electrodes as a function of [ProDOT **1**]/([ProDOT **1**]+[ProDOT-EO-Ester **2**]) ratio (Fig. S7c). C_{LF} is obtained from the impedance measurements, where the C_{LF} calculated from the imaginary part of the impedance (Z_{im}) diagram at the lowest frequency of 0.01 Hz and the C_{SP} calculated from the CV measurement at a scan rate of 50 mVs^{-1} polymer-coated electrodes vs. [ProDOT **1**]/[ProDOT **1** + PRODOT-EO-ester **2**] ratio (Fig. S7d) have a parallel trend. The findings indicate that feed ratio plays an important role on the composition of copolymer for the equal mole of ProDOT **1** and ProDOT-EO-ester **2,** resulting in an almost highest value in all charge, average surface coverage, a peak current density values, and capacitance.

Conclusions

Multilayer graphene sheets electro-coated with copolymers of ProDOT **1** and ProDOT-EO-ester **2** in this study with the aforementioned properties make them an attractive advanced functional material for supercapacitor, and battery applications. Morphologic, structural properties, and also, the capacitive performance of thin films of polymers on graphene structures reveal the unique dependence of this assembly on the electrical properties. As visualized from FEGSEM, the increase in the mole fraction of ProDOT-EO-ester **2** yields a denser, uniform and smooth surface. The AFM results are confirmed with the FEGSEM studies, where a low amount of monomer **2** containing CP1-1 and CP1-5 show similar morphology like PProDOT. The roughness of polymeric thin films decreases with an increasing component of ProDOT-EO-ester **2** in

copolymer films, presenting quite smooth and dense morphology in the case of CP1-25 and CP1-50. The shifting redox potential of copolymers to low value ensures an enhanced redox activity and capacitance properties, and altered morphologic features. By the increase of ProDOT in the copolymer composition, the higher dopant concentration is attained suggesting an enhanced redox activity, which correlates with the impedance and CV results. In addition, the specific capacitance is higher for the electrode prepared with equal molarities of both monomers indicating the best threshold for copolymerization. Moreover, the difference in the conjugated structure between ProDOT and ProDOT-EO-ester and the presence of the EO-ester group lead to a decrease in charge transfer resistance with the increasing mole fraction of the ProDOT-EO-ester. The E_{FB} and N_D values estimated from the linear part of the Mott-Schottky plots indicate the formation of a space charge layer at the semiconductor side. For the equal molar of initial feed ratio (CP1-1), the N_D was estimated as 2.25×10^{19} cm^{-3} and E_{FB} was 1.40 V, and for CP1-5 N_D was estimated as 9.70×10^{18} cm^{-3} and E_{FB} was 0.62 V, meaning that the corresponding values are shifted to lower positive values with the increasing mole fraction of the ProDOT-EO-ester. The variation in flat band potential of donor or acceptor density can be ascribed to the different interfaces between the polymer-coated samples and the electrolyte.

Acknowledgments

Support of the STSM via the COST Action CA15107 (MULTICOMP) for the short-term scientific mission at Erich Schmid Institute of Materials Science (ÖAW) to one of the authors (A.S.Sarac) is gratefully acknowledged. This work was supported by the European Research Council under the Advanced Grant "INTELHYB—Next generation of complex metallic materials in intelligent hybrid structures" (grant ERC-2013-ADG-340025). Fruitful discussions have been made with and technical help has been provided by M. Aydin.

ORCID

Tolga Karazehir https://orcid.org/0000-0002-2795-3675
Baran Sarac https://orcid.org/0000-0002-0130-3914
Jürgen Eckert https://orcid.org/0000-0003-4112-3181
A. Sezai Sarac https://orcid.org/0000-0001-7513-1740

References

1. Y. P. Zhai, Y. Q. Dou, D. Y. Zhao, P. F. Fulvio, R. T. Mayes, and S. Dai, *Adv. Mater.*, **23**, 4828 (2011).
2. H. L. Wang and H. J. Dai, *Chem. Soc. Rev.*, **42**, 3088 (2013).
3. A. Borenstein, O. Hanna, R. Attias, S. Luski, T. Brousse, and D. Aurbach, *J. Mater. Chem. A*, **5**, 12653 (2017).
4. D. B. Kong, X. Y. Qiu, B. Wang, Z. C. Xiao, X. H. Zhang, R. Y. Guo, Y. Gao, Q. H. Yang, and L. J. Zhi, *Sci. China Mater.*, **61**, 671 (2018).
5. C. J. Shearer, A. Cherevan, and D. Eder, *Adv. Mater.*, **26**, 2295 (2014).
6. L. S. Roselin, R. S. Juang, C. T. Hsieh, S. Sagadevan, A. Umar, R. Selvin, and H. H. Hegazy, *Materials*, **12**, 1229 (2019).
7. D. Seok, Y. Jeong, K. Han, D. Y. Yoon, and H. Sohn, *Sustainability-Basel*, **11**, 3694 (2019).
8. M. H. Al-Saleh, *Nanotechnology*, **30**, 062001 (2019).
9. R. Ciriminna, N. Zhang, M. Q. Yang, F. Meneguzzo, Y. J. Xu, and M. Pagliaro, *Chem. Commun.*, **51**, 7090 (2015).
10. L. J. A. Macedo, R. M. Iost, A. Hassan, K. Balasubramanian, and F. N. Crespilho, *Chemelectrochem*, **6**, 31 (2019).
11. D. A. C. Brownson, D. K. Kampouris, and C. E. Banks, *J. Power Sources*, **196**, 4873 (2011).
12. Y. Huang, J. J. Liang, and Y. S. Chen, *Small*, **8**, 1805 (2012).
13. Y. B. Tan and J. M. Lee, *J. Mater. Chem. A*, **1**, 14814 (2013).
14. X. H. Fan, B. D. Phebus, L. J. Li, and S. W. Chen, *Sci. Adv. Mater.*, **7**, 1916 (2015).
15. T. Palaniselvam and J. B. Baek, *2D Mater.*, **2**, 032002 (2015).
16. Q. Q. Ke and J. Wang, *J. Materiomics*, **2**, 37 (2016).
17. P. Sharma and T. S. Bhatti, *Energ. Convers. Manage*, **51**, 2901 (2010).
18. A. Davies and A. P. Yu, *Can. J. Chem. Eng.*, **89**, 1342 (2011).
19. F. Beguin, V. Presser, A. Balducci, and E. Frackowiak, *Adv. Mater.*, **26**, 2219 (2014).
20. S. X. Yan, S. H. Luo, J. Feng, P. W. Li, R. Guo, Q. Wang, Y. H. Zhang, Y. G. Liu, and S. Bao, *Chem. Eng. J.*, **381**, 122695 (2020).
21. R. Dubey and V. Guruviah, *Ionics*, **25**, 1419 (2019).
22. M. Jana, P. Khanra, N. C. Murmu, P. Samanta, J. H. Lee, and T. Kuila, *Phys. Chem. Chem. Phys.*, **16**, 7618 (2014).
23. D. W. Wang, F. Li, J. P. Zhao, W. C. Ren, Z. G. Chen, J. Tan, Z. S. Wu, I. Gentle, G. Q. Lu, and H. M. Cheng, *Acs Nano*, **3**, 1745 (2009).
24. X. M. Feng, R. M. Li, Y. W. Ma, R. F. Chen, N. E. Shi, Q. L. Fan, and W. Huang, *Adv. Funct. Mater.*, **21**, 2989 (2011).
25. S. Biswas and L. T. Drzal, *Chem. Mater.*, **22**, 5667 (2010).
26. S. Sahoo, G. Karthikeyan, G. C. Nayak, and C. K. Das, *Synthetic Met.*, **161**, 1713 (2011).
27. P. A. Mini, A. Balakrishnan, S. V. Nair, and K. R. V. Subramanian, *Chem. Commun.*, **47**, 5753 (2011).
28. F. Alvi, M. K. Ram, P. A. Basnayaka, E. Stefanakos, Y. Goswami, and A. Kumar, *Electrochim. Acta*, **56**, 9406 (2011).
29. C. Y. Chu, J. T. Tsai, and C. L. Sun, *Int. J. Hydrogen Energ.*, **37**, 13880 (2012).
30. Y. Chen, J. H. Xu, Y. J. Yang, S. B. Li, W. Y. Yang, T. J. Peng, X. L. Mao, and Y. T. Zhao, *J. Mater. Sci-Mater. El.*, **26**, 8292 (2015).
31. D. Jacob, P. A. Mini, A. Balakrishnan, S. V. Nair, and K. R. V. Subramanian, *B Mater. Sci.*, **37**, 61 (2014).
32. Y. Su, S. H. Qiu, Y. Liu, D. P. Yang, H. C. Zhao, and L. P. Wang, *Int. J. Electrochem. Sc.*, **14**, 4595 (2019).
33. D. Gulercan, I. Gergin, and A. S. Sarac, *Fiber Polym.*, **19**, 2178 (2018).
34. M. C. Yang, H. M. Tsou, Y. S. Hsiao, Y. W. Cheng, C. C. Liu, L. Y. Huang, X. Y. Peng, T. Y. Liu, M. C. Yung, and C. C. Hsu, *Polymers-Basel*, **11**, 1520 (2019).
35. T. T. Tung, M. Castro, J. F. Feller, T. Y. Kim, and K. S. Suh, *Org. Electron.*, **14**, 2789 (2013).
36. B. L. Groenendaal, F. Jonas, D. Freitag, H. Pielartzik, and J. R. Reynolds, *Adv. Mater.*, **12**, 481 (2000).
37. S. Kirchmeyer and K. Reuter, *J. Mater. Chem.*, **15**, 2077 (2005).
38. J. L. Niu, L. M. Rao, P. Liu, W. W. Zhang, W. N. Zhang, Y. X. Zuo, K. K. Chai, S. Chen, J. K. Xu, and X. M. Duan, *Synthetic Met.*, **246**, 282 (2018).
39. X. Strakosas, B. Wei, D. C. Martin, and R. M. Owens, *J. Mater. Chem. B*, **4**, 4952 (2016).
40. E. Unur, P. M. Beaujuge, S. Ellinger, J. H. Jung, and J. R. Reynolds, *Chem. Mater.*, **21**, 5145 (2009).
41. X. M. Chen, J. Y. Zhang, and M. D. Yang, *J. Mater. Sci-Mater. El.*, **29**, 16469 (2018).
42. M. D. Damaceanu, H. D. Gilsing, B. Schulz, A. Arvinte, and M. Bruma, *RSC Adv.*, **4**, 52467 (2014).
43. P. Blanchard, L. Huchet, E. Levillain, and J. Roncali, *Electrochem. Commun.*, **2**, 1 (2000).
44. A. S. Sarac, H. D. Gilsing, A. Gencturk, and B. Schulz, *Prog. Org. Coat.*, **60**, 281 (2007).
45. A. S. Sarac, A. Gencturk, H. D. Gilsing, B. Schulz, and C. M. Turhan, *J. Nanosci. Nanotechno.*, **9**, 2877 (2009).
46. A. S. Sarac, S. E. Ozgul, A. Gencturk, B. Schulz, H. D. Gilsing, and H. Faltz, *Prog. Org. Coat.*, **69**, 527 (2010).
47. A. S. Sarac, S. E. Ozgul, H. Faltz, A. Gencturk, H. D. Gilsing, and B. Schulz, *J. Nanosci. Nanotechno.*, **10**, 8043 (2010).
48. M. R. Rosario-Canales, P. Deria, M. J. Therien, and J. J. Santiago-Aviles, *Acs Appl. Mater. Inter.*, **4**, 102 (2012).
49. M. C. Turhan, A. S. Sarac, A. Gencturk, H. D. Gilsing, H. Faltz, and B. Schulz, *Synthetic Met.*, **162**, 511 (2012).
50. F. G. Guler, H. D. Gilsing, B. Schulz, and A. S. Sarac, *J. Nanosci. Nanotechno.*, **12**, 7869 (2012).
51. M. G. Ersozoglu, H. D. Gilsing, A. Gencturk, and A. S. Sarac, *Int. J. Electrochem. Sc.*, **14**, 9504 (2019).
52. L. R. Savagian, A. M. Osterholm, J. F. Ponder, K. J. Barth, J. Rivnay, and J. R. Reynolds, *Adv. Mater.*, **30**, 1804647 (2018).
53. A. W. Lang, J. F. Ponder, A. M. Osterholm, N. J. Kennard, R. H. Bulloch, and J. R. Reynolds, *J. Mater. Chem. A*, **5**, 23887 (2017).
54. J. Wang, W. X. Lv, J. H. Wu, H. Y. Li, and F. Li, *Anal. Chem.*, **91**, 13831 (2019).
55. H. H. Zhou, X. M. Zhi, W. Y. Zhang, and H. J. Zhai, *Org. Electron.*, **69**, 98 (2019).
56. B. A. Abd-El-Nabey, O. A. Abdullatef, and R. M. Salman, *Int J Corros Scale I*, **7**, 62 (2018).
57. Z. M. He, J. Liu, S. Y. Khoo, and T. T. Y. Tan, *ChemSusChem*, **9**, 172 (2016).
58. M. Besbes, G. Trippe, E. Levillain, M. Mazari, F. Le Derf, I. F. Perepichka, A. Derdour, A. Gorgues, M. Salle, and J. Roncali, *Adv. Mater.*, **13**, 1249 (2001).
59. P. Marrec, B. Fabre, and J. Simonet, *J. Electroanal. Chem.*, **437**, 245 (1997).
60. L. H. Shi, F. Garnier, and J. Roncali, *Macromolecules*, **25**, 6425 (1992).
61. J. Roncali, R. Garreau, D. Delabouglise, F. Garnier, and M. Lemaire, *J. Chem. Soc. Chem. Comm.*, 679 (1989).
62. C. Y. Hsu, H. W. Chen, K. M. Lee, C. W. Hu, and K. C. Ho, *J. Power Sources*, **195**, 6232 (2010).
63. Y. Chen, J. H. Xu, Y. W. Mao, Y. J. Yang, W. Y. Yang, and S. B. Li, *Mater. Sci. Eng. B-Adv.*, **178**, 1152 (2013).
64. J. D. Stenger-Smith, C. K. Webber, N. Anderson, A. P. Chafin, K. K. Zong, and J. R. Reynolds, *J. Electrochem. Soc.*, **149**, A973 (2002).
65. M. Gholami, P. M. Nia, L. Narimani, M. Sokhakian, and Y. Alias, *Appl. Surf. Sci.*, **378**, 259 (2016).
66. M. Gholami, P. M. Nia, and Y. Alias, *Appl. Surf. Sci.*, **357**, 806 (2015).
67. C. W. Kuo, T. L. Wu, Y. C. Lin, J. K. Chang, H. R. Chen, and T. Y. Wu, *Polymers-Basel*, **8**, 15 (2016).
68. T. Karazehir, M. Ates, and A. S. Sarac, *J. Electrochem. Soc.*, **163**, G107 (2016).
69. H. G. Wei, H. B. Gu, J. Guo, S. Y. Wei, and Z. H. Guo, *J. Electrochem. Soc.*, **160**, G3038 (2013).
70. Y. Sulaiman and R. Kataky, *J. Electrochem. Soc.*, **159**, S8 (2012).

71. E. Ismar, T. Karazehir, M. Ates, and A. S. Sarac, *J. Appl. Polym. Sci.*, **135**, 45723 (2018).
72. S. B. Singh, T. Kshetri, T. I. Singh, N. H. Kim, and J. H. Lee, *Chem. Eng. J.*, **359**, 197 (2019).
73. K. U. Lee, J. Y. Byun, H. J. Shin, and S. H. Kim, *J. Alloy. Compd.*, **779**, 74 (2019).
74. T. C. An, Y. Z. Ling, S. Gong, B. W. Zhu, Y. M. Zhao, D. S. Dong, L. W. Yap, Y. Wang, and W. L. Cheng, *Adv. Mater. Technol-Us.*, **4**, 1800473 (2019).
75. J. Rodriguez-Moreno, E. Navarrete-Astorga, E. A. Dalchiele, R. Schrebler, J. R. Ramos-Barrado, and F. Martin, *Chem. Commun.*, **50**, 5652 (2014).
76. R. Jamal, L. Zhang, M. C. Wang, Q. Zhao, and T. Abdiryim, *Prog. Nat. Sci-Mater.*, **26**, 32 (2016).
77. A. Ali, R. Jamal, W. W. Shao, A. Rahman, Y. Osman, and T. Abdiryim, *Prog. Nat. Sci-Mater.*, **23**, 524 (2013).
78. Y. J. Hu, D. F. Hu, S. L. Ming, X. M. Duan, F. Zhao, J. Hou, J. K. Xu, and F. X. Jiang, *Electrochim. Acta*, **189**, 64 (2016).
79. B. Duran and G. Bereket, *Ind. Eng. Chem. Res.*, **51**, 5246 (2012).
80. C. M. Santos, M. C. R. Tria, R. Vergara, F. Ahmed, R. C. Advincula, and D. F. Rodrigues, *Chem. Commun.*, **47**, 8892 (2011).
81. E. Tamburri, S. Orlanducci, F. Toschi, M. L. Terranova, and D. Passeri, *Synthetic Met.*, **159**, 406 (2009).
82. L. Zhang, R. Jamal, Q. Zhao, Y. Zhang, M. C. Wang, and T. Abdiryim, *Polym. Composites*, **37**, 2884 (2016).
83. C. R. Siju, T. R. Saravanan, K. N. Rao, and S. Sindhu, *Int. J. Polym. Mater. Po.*, **63**, 374 (2014).
84. C. B. Nielsen and T. Bjornholm, *Macromolecules*, **38**, 10379 (2005).
85. M. S. Cho, S. Y. Kim, J. D. Nam, and Y. Lee, *Synthetic Met.*, **158**, 865 (2008).
86. F. G. Guler and A. S. Sarac, *Express Polym. Lett.*, **5**, 493 (2011).
87. U. S. Waware, G. J. Summers, M. Rashid, and A. M. S. Hamouda, *Ionics*, **24**, 1701 (2018).
88. Q. Bricaud, A. Cravino, P. Leriche, and J. Roncali, *Sol. Energ. Mat. Sol. C*, **93**, 1624 (2009).
89. M. A. del Valle, L. I. Canales, A. Ramos, F. R. Diaz, L. A. Hernandez, F. Armijo, J. C. Bernede, L. Cattin, and G. Louarn, *Int J Electrochem Sc*, **8**, 1422 (2013).
90. T. Wagner, J. Lazar, U. Schnakenberg, and A. Boker, *Acs Appl. Mater. Inter.*, **8**, 27282 (2016).
91. Z. S. Zhao and P. G. Pickup, *J. Chem. Soc. Faraday T*, **90**, 3097 (1994).
92. P. K. Kathuroju and J. Nagaraju, *Micro. Nano. Lett.*, **6**, 1002 (2011).
93. A. Charron, C. Esnault, Z. Abada, C. Marcel, B. Schmaltz, and F. Tran-Van, *Polym. Int.*, **67**, 684 (2018).
94. A. Parsa and S. A. Salout, *J. Electroanal. Chem.*, **760**, 113 (2016).
95. B. Muthulakshmi, D. Kalpana, S. Pitchumani, and N. G. Renganathan, *J. Power Sources*, **158**, 1533 (2006).
96. W. C. Chen, T. C. Wen, C. C. Hu, and A. Gopalan, *Electrochim. Acta*, **47**, 1305 (2002).
97. J. C. Byers, P. M. DiCarmine, M. M. A. Moustafa, X. Wang, B. L. Pagenkopf, and O. A. Semenikhin, *J. Phys. Chem. B*, **113**, 15715 (2009).
98. C. V. Krishnan and M. Garnett, *Int. J. Electrochem. Sc.*, **1**, 283 (2006).
99. J. Gasiorowski, A. I. Mardare, N. S. Sariciftci, and A. W. Hassel, *J. Electroanal. Chem.*, **691**, 77 (2013).